Biphenyl Au(III) Complexes with Phosphine Ancillary Ligands: Synthesis, Optical Properties, and Electroluminescence in Light-Emitting Electrochemical Cells

Jeannine Yang, Valerio Giuso, Min-Chih Hou, Edwyn Remadna, Jérémy Forté, Hai-Ching Su, Christophe Gourlaouen, Matteo Mauro, Benoît Bertrand

Biphenyl Au(III) complexes with phosphine ancillary ligands: synthesis, optical properties and electroluminescence in light-emitting electrochemical cells

Jeannine Yang,[a]‡ Valerio Giuso,[b]‡ Min-Chih Hou,[c] Edwyn Remadna,[a] Jérémy Forté,[a] Hai-Ching Su,[c] Christophe Gourlaouen,[d] Matteo Mauro,[b]* Benoît Bertrand[a]**

a Sorbonne Université, CNRS, Institut Parisien de Chimie Moléculaire (IPCM UMR 8232), F-75005 Paris, France

b Université de Strasbourg & CNRS, Institut de Physique et Chimie des Matériaux de Strasbourg (IPCMS UMR 7504), F-67034 Strasbourg, France

c Institute of Lighting and Energy Photonics, National Yang Ming Chiao Tung University, Tainan 71150, Taiwan

d Université de Strasbourg, CNRS, Institut de Chimie de Strasbourg, UMR 7177, Laboratoire de Chimie Quantique, 4 rue Blaise Pascal, 67081 Strasbourg, France

KEYWORDS: Gold complexes, diphosphine ligands, metalated ligands, luminescence, density-functional theory, light-emitting electrochemical cells

ABSTRACT: A series of ten cationic complexes of general formula [(C^C)Au(P^P)]X, where C^C = 4,4'-di-tert-butyl-1,1'-biphenyl, P^P is a diphosphine ligand and X is a non-coordinating counter-anion, has been synthesized and fully characterized by means of chemical and X-ray structural methods. All the complexes display a remarkable switch-on of the emission properties when going from fluid solution to solid state. In this latter, long-lived emission with lifetime τ = 1.8–83.0 μs and maximum in the green-yellow region is achieved with moderate to high photoluminescence quantum yield (PLQY). This emission is ascribed to an excited-state with mainly triplet ligand-centered (^{3}LC) nature. This effect strongly indicates that rigidification of the environment helps to suppress non-radiative decay, which is mainly attributed to the large molecular distortion in the excited state, as supported by density functional theory (DFT) and time-dependent DFT (TD-DFT) computation. In addition, quenching intermolecular interactions of the emitter are avoided thanks to the steric hindrance of the substituents. Emissive properties are therefore restored efficiently. The influence of both diphosphine and anion have been investigated and rationalized as well. Using two complexes as examples and owing to their enhanced optical properties in the solid state, the first proof-of-concept of the use of gold(III) complexes as electroactive materials for the fabrication of light-emitting electrochemical cell (LEC) devices is herein demonstrated. The LECs achieve peak external quantum efficiency, current efficiency, and power efficiency up to *ca.* 1%, 2.6 cd A^{-1}, and 1.1 lm W^{-1}, for complex **1PF$_6$** and 0.9%, 2.5 cd A^{-1}, and 0.7 lm W^{-1}, for complex **3**, showing the potential use of these novel emitters as electroactive compounds in LEC devices.

Introduction

Light-emitting electrochemical cells (LECs) are optoelectronic devices that are attracting a growing attention in the recent years due to their potential application in large-area and low-cost display technology.[1–4] LECs consist of a layer of a light-emitting material sandwiched between a low work function metal cathode and a transparent anode (typically indium tin oxide, ITO). Owing to their easier, solution-processed fabrication and overall simpler architecture that employ air-stable cathodes, LECs are considered a valuable alternative to more expensive organic light-emitting diode (OLED) technology. However, the device efficiency and lifetime of LECs are still inferior to OLEDs. Especially, blue emitters for LECs are much less stable and efficient than those with lower energy gap. In addition, dynamically extending doped layers also affects the device stability of LECs. Irreversible electrochemical reactions in charge transporting are suggested to be responsible for the reduced lifetime of blue LECs.[5] One of the feasible approaches to improve the device stability is incorporating carrier-transporting materials into the emissive layer.[6,7] Therefore, the blue emitters are free from transporting of charge carriers, rendering better electrochemical stability. Tailoring carrier balance to reach centred recombination zone improves not only the device efficiency but also the device stability.[8,9] Optimizing driving mode is another feasible way to improve the device stability. Pulsed-current driving for LECs has been shown to offer superior device stability than constant-voltage and constant-current driving.[10] With these continuously developing technologies to improve device performance, simple solution-processable fabrication, advantages of great tolerance to emissive-layer thickness, substrate roughness, and electrode work function render LECs competitive in low-cost light sources for flexible displays.

LEC operating mechanism requires mobile ions to form the electrochemical *p*-i-*n* junction upon the application of a suitable electrical bias. Hence, ionic transition metal complexes (iTMCs) are typically employed as electroluminescent materials in LECs where they act as both charge carriers

and photoactive compounds. Undoubtedly, cyclometalated iridium(III)-based iTMCs play a leading role in the field and they warrant efficient both singlet and triplet excitons harvesting,[11] although examples involving Pt(II),[12] Ru(II)[13] and Cu(I)[14,15] are also reported. Since the first report on the iridium-based LEC in 2004,[16] Ir(III) complexes have been shown to be the most promising candidates among other iTMCs.[17] A wide variety of LECs employing iridium complexes delivering blue, green, yellow, orange, red, near infrared (NIR), and white emission have been published. With judicious molecular design and device engineering, some reported iridium-based LECs have reached high external quantum efficiencies (EQEs) up to or higher than 20%.[18–21] The ruthenium complex was the first iTMC used for LECs,[22] but the ruthenium-based LECs generally showed red to NIR electroluminescence (EL) spectra and the maximum EQEs were around only 1%.[23] The LECs employing a Pt porphyrin,[24] a Pt(II) dimer,[25] and a dinuclear Ir(III)/Pt(II) complex[26] exhibited red to NIR EL and the maximum EQE achieved with the host-guest strategy was up to 2.7%.[26] The EL from the platinum-based LECs turned into green when the carbazole-appended carbene ligand was utilized.[27] Recently, copper complexes have attracted much research attention due to their relatively higher abundance than other iTMCs in Earth's crust.[28] A high EQE up to 16% was achieved in the LECs based on a copper complex.[29] The use of other metal complexes is much less explored and largely overlooked to date, yet highly sought. Surprisingly, no example reports on the use of luminescent gold complexes in LECs, to the best of our knowledge.

The chemistry of gold compounds mainly involves the +I oxidation state of the metal centre;[30] whereas complexes featuring gold in its +III valency are less common.[31] This is because the synthesis of these latter requires harsh synthetic conditions and strong donor ligands to improve the chemical stability of the resulting complexes and suppress their tendency towards reduction.

Despite this, gold(III) complexes are attracting an increasing interest in the recent past driven by their emerging applications as active compounds in several fields including antitumoral[32,33] and antiviral agents in medicine,[34] catalysis[35] and, more recently, as emitters in OLEDs.[36]

Achieving satisfactory emission properties in gold(III) complexes requires strict conditions. Firstly, the high oxidation potential that characterizes gold(III) complexes pulls HOMO levels deep down and pushes typically radiative metal-to-ligand charge transfer (MLCT) states to much higher energy compared to the widely investigated d^8 Pt(II) counterparts. As consequence, the photochemistry and photophysics of gold(III) complexes is often detrimentally dominated by energetically low-lying states with metal-centred (*d-d*) and/or ligand-to-metal charge transfer (LMCT) character that can be easily populated. Secondly, their square-planar geometry is prone to D_{2d} geometrical distortion of the excited state and greatly favour the establishment of intermolecular interactions.

Overall, these features make easily available radiationless relaxation pathways back to the electronic ground state. Hence, the vast majority of Au(III) complexes display no luminescence in either solution or solid state. Luminescent gold(III) derivates with efficient emission properties requires judicious chemical design of the coordination sphere of the metal and their synthesis is still particularly challenging.

Yam and co-workers firstly reported on the photoluminescence in stable Au(III) complexes at room temperature by employing ligand design strategies based on strong σ-donating ligands.[37,38] The same group further extended such strategies demonstrating the use of C-based *bis*-cyclometalated Au(III) complexes as emitters in organic light-emitting devices. These complexes feature alkynyl to phenylpyridine electron density displacement with ligand-to-ligand charge

transfer (LLCT) states.[39] More recently, biphenyl Au(III) complexes have been investigated in fundamental organometallic chemistry,[40,41] catalysis,[42,43] photoluminescence[44–46] and biology.[47]

Achieving fine control of the supramolecular aggregation and effectively managing with intermolecular interactions is of paramount importance for avoiding significant spectral broadening and improving device performances in particular when high concentration of electroluminescent dopant is required, as it would be in the case of LEC devices. The management of intermolecular interactions can be particularly cumbersome for square-planar complexes, such as Au(III) complexes, that have high tendency to establish intermolecular interactions via π-π stacking as well as to phase segregate due to strong aggregation, with detrimental implications for both optical properties and device outputs. Increase of the steric hindrance has shown to be a suitable way to improve emitter processability, limit its aggregation and related quenching phenomena in light-emitting devices.[2,48]

We herein aim at efficiently suppressing intermolecular interactions in luminescent biphenyl Au(III) complexes in view of their use in optoelectronics. The synthesis, structural, electrochemical and photophysical properties of a series of cationic *bis*-chelated Au(III) complexes are therefore comprehensively presented. The compounds possess general formula $[Au(C\hat{}C)(P\hat{}P)]^+$, where C^C is a biphenyl chromophoric ligand and P^P is a chelating diphosphine. Remarkably, these complexes display photoluminescence in the solid state with quantum yield up to 0.39, and the effect of the nature of the P^P ligand and counterion onto the photophysical properties are investigated in detail. Their optical properties are further elucidated by means of computational investigation at (TD)-DFT level that helped to provide fundamental insights on the lack of photoluminescence in solution at room temperature. Finally, the most

promising compounds have been tested as emitters in proof-of-concept LEC devices, which is unprecedented for Au(III) compounds.

Results and discussion

Synthesis and characterization

The mononuclear cationic [(C^C)Au(P^P)]X complexes **1**–**5** were synthesized by the reaction of two equivalents of the corresponding diphosphine ligands with a $[(C^C)AuCl]_2$ dimer under N_2 atmosphere to prevent diphosphine oxidation, followed by anion metathesis using either potassium or silver salts. The overall synthetic strategy was adapted from a previously reported protocols.[45,47] In both cases, only the cationic mononuclear complexes with the corresponding chelating diphosphine were obtained in good yields (Scheme 1). The formation of the mononuclear structures was assessed by ^{1}H NMR showing only one set of symmetrical signals for both the (C^C) and (P^P) ligands in a 1:1 ratio. Moreover, the signal of H^2 (see Scheme 1 for labelling) appeared between 7.10 and 7.30 ppm thus more shielded than in $[(C^C)Au(N^N)]BF_4$ complexes (δH^2 between 7.50 and 7.60 ppm).[47] This shift is due to the shielding cone of the phenyl groups of the PPh_2 ligands in *cis* position with respect to the aryl ligand. Moreover, these signals appear with a strong $^3J_{P\text{-}H}$ coupling constant of 8 Hz demonstrating the coordination of the diphosphines onto the $[(C^C)Au]^+$ moiety. In the same way, the $^{31}P\{^1H\}$ NMR spectra of the different complexes showed a single singlet signal for the two phosphorous atoms of the (P^P) ligands deshielded with respect to the corresponding diphosphines.

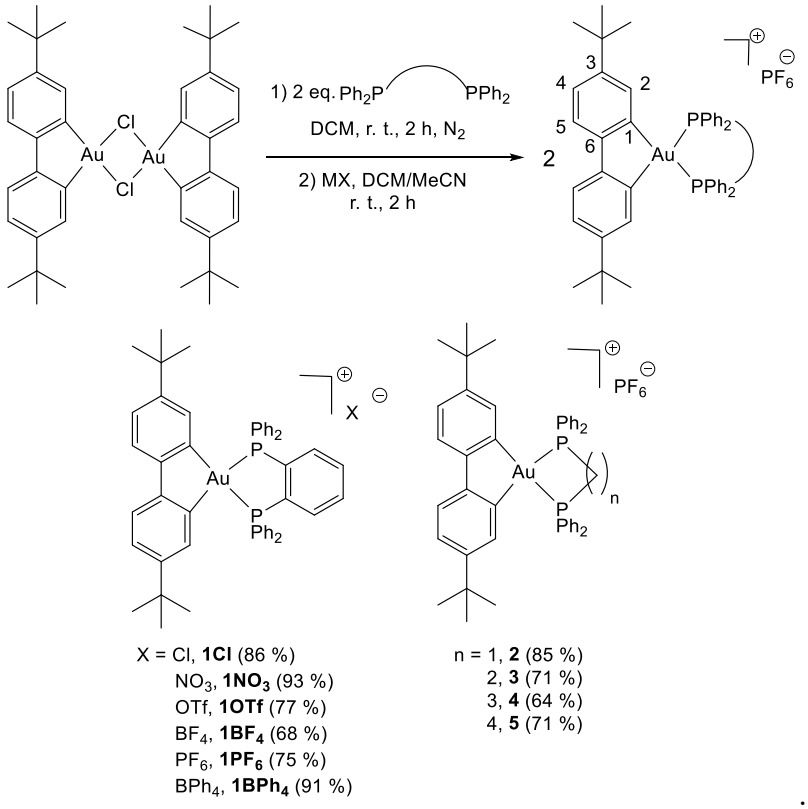

Scheme 1. Synthetic variation of the chelating diphosphine ligand and counteranion.

In order to estimate the impact of the charge on the structures and of the Au(III) cation in the photoluminescence properties, a dicationic Au(III) and a monocationic Pt(II) complexes were synthetized for sake of comparison. The [(C^N)Au(P^P)]$(PF_6)_2$ complex **6** was synthetized by the reaction of the corresponding [(C^N)$AuCl_2$] with diphenylphosphinoethane (dppe) followed by the abstraction of the two chlorides by a silver salt according to a protocol established by Cinellu and colleagues affording **6** in excellent yield (Scheme 2).[49] The [(C^N)Pt(P^P)]PF_6 complex **7** was synthetized by the reaction of the [(C^N)Pt(DMSO)Cl] precursor with diphenylphosphinoethane followed by the abstraction of the chlorido ligand by a silver salt following a reported procedure leading to the isolation of **7** in excellent yield (Scheme 2).

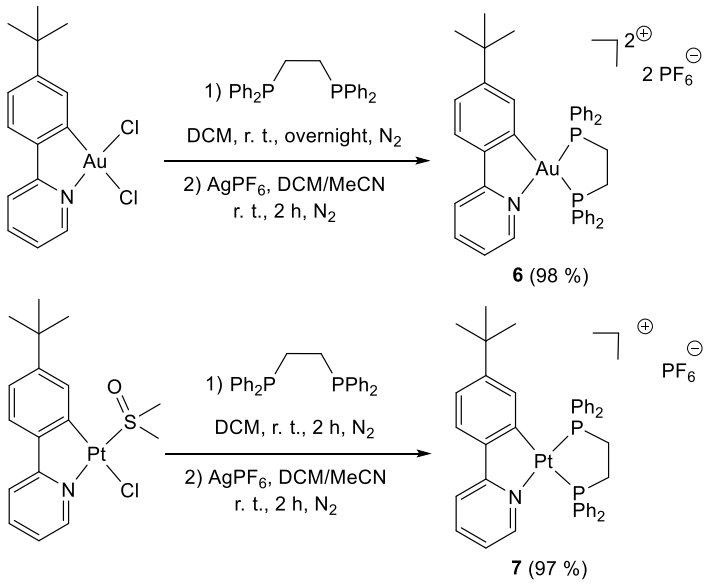

Scheme 2. Schematic synthetic pathway employed for the synthesis of complexes **6** and **7**.

The formation of **6** and **7** was assessed by $^{31}P\{^{1}H\}$ that showed two sets of signals integrating for one each due to the presence of the unsymmetrical (C^N) chelating ligand. Furthermore, in the case of **7**, two different $^{1}J_{Pt\text{-}P}$ coupling constants of 1830 and 3780 Hz corresponding to the P in *trans* position with respect to the C and N respectively, were observed. This corresponds to the data obtained for similar complexes.[50] The ^{1}H NMR spectra of **6** and **7** also showed the expected 1:1 ratio between the (C^N) and (P^P) ligands.

Solid state structures

Single crystals suitable for X-ray diffraction were grown by slow evaporation of a solution in a mixture DCM/petroleum ether (**1Cl** and **2–5**), DCM/toluene (**1PF$_6$**), and chloroform (**7**). The crystal structures are depicted in Figure 1 and S1–S4 of the ESI. For all the complexes, the crystallographic data unambiguously confirmed the expected structures. All the complexes present the typical four-coordinated square-planar geometry of the Au(III) and Pt(II) cations with small

distortions due to the bite angle of the (C^C), (C^N) and (P^P) chelates. As one could have expected, the smaller the spacer between the two PPh_2 moieties the sharper the P_1–M–P_2 angle. Indeed, in complex **2** with a diphenyphosphinomethane (dppm) ligand the P_1–Au–P_2 angle has a value of 69.8° while the same angle in complex **5** with a diphenyphosphinobutane (dppb) ligand has a value of 95.1° (Table 1). However, these differences in metallacycle tension did not affect the Au–P bond length as for all complexes both Au–P bonds appeared to have similar length around 2.39 Å. Moreover, it appeared that the P_1–M–P_2 value seems to be influenced only by the number of carbons between the PPh_2 ligands and not by the nature of the linker (alkyl or aryl) or the coordinated metal (Au or Pt) as can be seen for complexes **1Cl**, **PF_6**, **3** and **7** that all show a P_1–M–P_2 angle between 80.2 and 84.4° (Table 1).

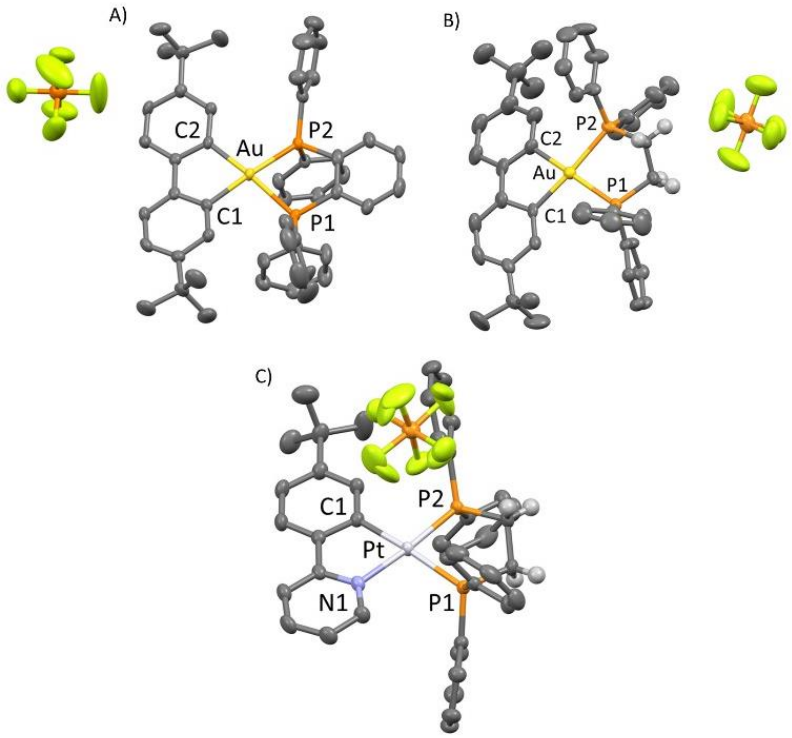

Figure 1. A) Crystal structure of one complex of the asymmetric unit of **1PF_6**. Ellipsoids set at 50% probability. Hydrogen atoms and toluene have been omitted for clarity. Selected bond

distances [Å] and angles [°] measured at 200 K: Au–P_1 2.3901(12), Au–P_2 2.3866(12), Au–C_2 2.086(5), Au–C_1 2.084(5), P_1–Au–P_2 81.28(4), P_2–Au–C_2 98.55(13), C_2–Au–C_1 80.72(18), C_2–Au–P_1 98.49(13). B) Crystal structure of complex **3**. Ellipsoids set at 50% probability. Minor position of complex is omitted for clarity. Only hydrogens atoms involved in the $P(CH_2)_2P$ bridge are depicted. Selected bond distances [Å] and angles [°] measured at 200 K: Au–P_1 2.3637(16), Au–P_2 2.3760(16), Au–C_1 2.074(6), Au–C_2 2.077(6), P_1–Au–P_2 84.38(6), P_2–Au–C_2 98.63(17), C_2–Au–C_1 81.5(2), C_2–Au–P_1 95.78(19). C) Crystal structure of complex **7**. Ellipsoids set at 50% probability. PF_6 anion is disordered over two positions with an occupancy rate of 60/40. Chloroform molecules have been omitted for clarity. Only hydrogens atoms involved in the $P(CH_2)_2P$ bridge are depicted. Selected bond distances [Å] and angles [°] measured at 200 K: Pt–P_1 2.3175(6), Pt–P_2 2.2350(5), Pt–C_1 2.063(2), Pt–N 2.1048(19), P_1–Pt–P_2 84.43(2), P_2–Pt–C_1 96.69(7), C_1–Pt–N 80.03(8), N–Pt–P_1 99.15(6).

Table 1. Selected geometric data for monomeric complexes **1Cl**, **1PF$_6$**, **2-5** and **7** measured by X-ray diffractometric analysis.

Complex	M–P_1 bond length [Å]	M–P_2 bond length [Å]	P_1–M-P_2 angle [°]
1Cl	2.3871(8)	2.3897(8)	80.17(3)
1PF$_6$	2.3901(12)	2.3866(12)	81.28(4)
2	2.399(3)	2.401(3)	69.84(11)
3	2.3637(16)	2.3760(16)	84.38(6)
4	2.3814(7)	2.3811(8)	89.14(3)
5	2.3926(8)	2.3970(8)	95.11(3)

7	2.3175(6)	2.2350(5)	84.43(2)

Photophysical investigation

Firstly, the archetypal complex **1PF$_6$** was investigated in dilute CH_3CN solution at room temperature. The corresponding spectrum is displayed in Figure 2 and the data are listed in Table 2. The intense ($\varepsilon = 5.25\times10^4$ M^{-1} cm^{-1}) high-energy band at λ_{abs} = *ca.* 262 nm is ascribed to a singlet intraligand (^{1}IL) transition with π–π* nature involving the biphenyl moiety, in accordance with the spectrum of the biphenylene proligand,[51] and with fact that it is little dependent on the nature of the ancillary diphosphine ligand. At longer wavelengths the lower intensity band ($\varepsilon = 5.0\times10^3$ M^{-1} cm^{-1} at λ_{abs} = 318 nm) can be ascribed to a singlet-manifold electronic transition with mainly metal perturbed ligand-to-ligand charge transfer (^{1}LLCT) and ligand-to-metal charge transfer (^{1}LMCT) character. The CT character of this latter band is corroborated by the bathochromic shift observed upon increasing solvent polarity (see Table S2 and Figure S5). Overall, this band attribution is in agreement with those reported previously for related complexes[44,45,51] and with the computational data (see below). For this class of chromophores, singlet metal-to-ligand charge transfer (^{1}MLCT) states are expected to lie at much higher energy compared to related cyclometalated square-planar platinum(II) complexes due to the higher oxidation potential of the gold atom in its +III valency when compared to the former. This is indeed confirmed by analysing the spectral feature of complex **7** that displays a more intense band in the region at 330 nm with ^{1}MLCT character (see Figure 2). On the other hand, the higher intensity of the band at 310 nm observed for the related complex **6** can be ascribed to a transition with admixed intraligand charge transfer (^{1}ILCT) and ^{1}LLCT character (see Figure 2).

The anion seems to exert little effect on both energy and intensity of the electronic absorption bands as shown in Figure 2 and S6 of the ESI. Similarly, variation of the diphenylphosphine seems to have a little impact on the absorption spectral feature and the comparison of the UV-visible spectra for derivative **1PF$_6$** and **2**–**5** is displayed in Figure 2. See Table 1 for data.

No detectable emission was observed for any of the samples in solution when recorded in either air-equilibrated or degassed condition upon irradiation in the range λ_{exc} = 260–320 nm. This finding is indicative of the very efficient non-radiative deactivation channels in solution, and it is in agreement with data on related [(C^C)Au(L^L)]$^+$ derivatives reported previously.[45] The lack of emission is most likely due to the rapid thermal population of quenching d-d states that takes place at room temperature as well as to high degree of structural distortion occurring at the excited states that favours efficient non-radiative vibrational coupling with the electronic ground state.

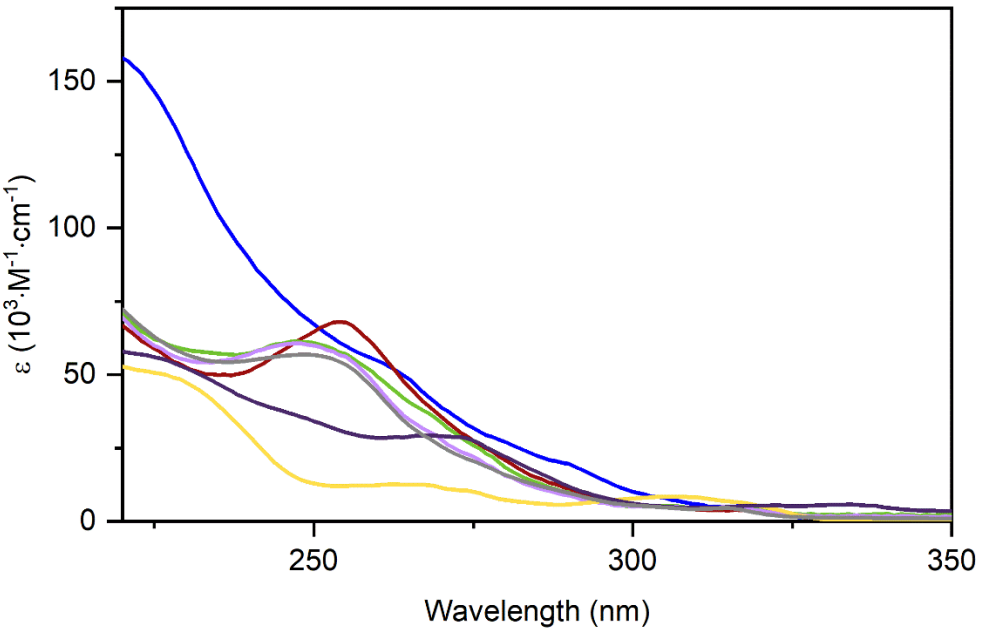

Figure 2. Electronic absorption spectra in the UV region in diluted CH_3CN at room temperature. Compounds **1PF$_6$** (blue), **2** (brown), **3** (green), **4** (lilac), **5** (grey), **6** (yellow) and **7** (purple).

Lowering the temperature is expected to efficiently reduce population of thermally accessible quenching states, vibrational motion and structural distortion, thus restoring the emission properties from the lowest-lying state radiative deactivation. For all the derivatives, going from room temperature to glassy matrix at 77 K in 2-MeTHF is accompanied by the appearance of intense photoluminescence indeed. The corresponding emission spectra are displayed in Figure 3, S7 and S8 of the ESI and the data tabulated in Table 2. Low temperature emission spectra display a structured profile in the blue-green region with vibronic progression of spacing in the range 1500–1250 cm^{-1} that can be with confidence ascribed to the stretching modes of aromatic scaffolds and are in agreement with intramolecular vibrational modes observed for the biphenyl (1050–1275 cm^{-1}).[44,45] Time-resolved emission decays shows (average) excited-state lifetime in the order of 30–148 μs for all the Au(III) derivatives investigated, corroborating the formally triplet nature of the emitting state with mainly ^{3}IL character ($T_1 \rightarrow S_0$ transition).

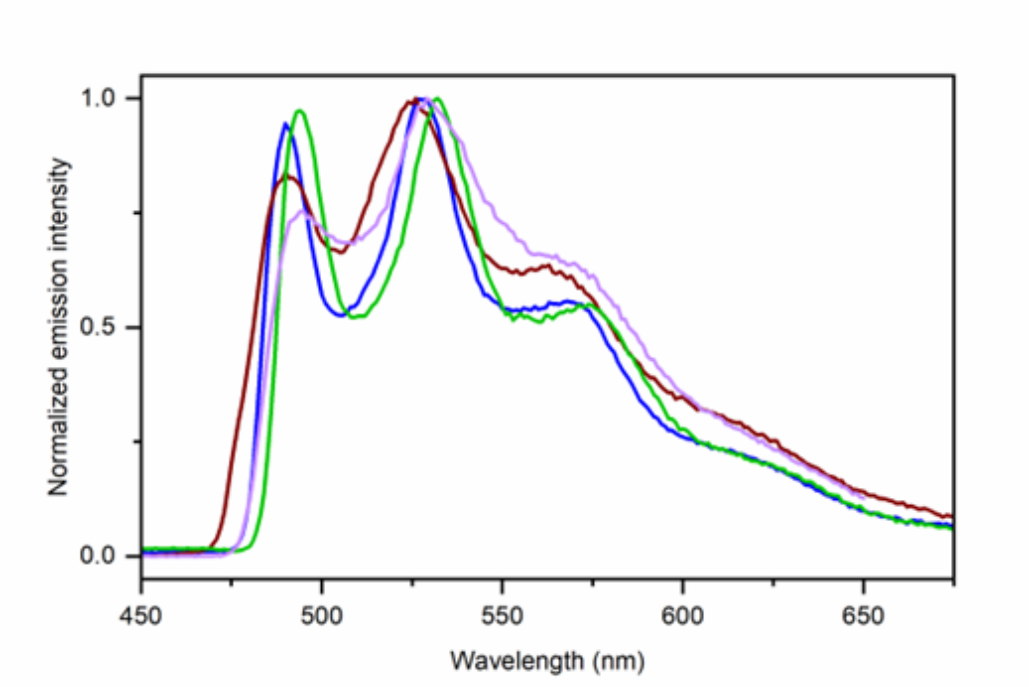

Figure 3. Emission spectra in 2-MeTHF glassy matrix at 77 K upon excitation at λ_{exc} = 360 nm. Compounds **1PF$_6$** (blue), **2** (brown), **3** (green) and **4** (lilac).

Rigidification of the environment at room temperature helps in restoring the emission properties as well. Indeed, remarkable switch-on of the photoluminescence is observed in the solid-state sample for all the derivatives. Such enhancement of the emission properties is most likely due to the reduced structural distortion and population of quenching excited states that would act as efficient radiationless pathways. A slow irradiation time-dependent decomposition is observed for compound **2** and, to a minor extent, derivative **5** in the solid state attributable to the non-optimal bite angle of diphenylphosphinomethane (dppm) and diphenylphosphinobutane (dppb) ligands that reduces chemical stability. The complete set of photophysical data recorded for samples in the solid-state as neat powder is listed in Table 3 and the emission spectra are displayed in Figure 4–5.

In sharp contrast with optical data in solution, the nature of the counterion clearly exerts a major effect on the photoluminescence properties of these emitters in the solid state (see Figure 4 for comparison of emission spectra of complexes of series **1**). The nature of the counterion seems to influence the emission spectra both in terms of wavelength and spectral profile. It is reasonable to think that the crystal packing and the soft vs. hard nature of the anion influences the local polarity of the microenvironment around the Au(III) emitters. Thus, the counterion is playing a role in the stabilization of the lower-lying ^{1,3}CT excited state and, in turn, the mixing of these latter with the emitting ^{3}IL state. Amongst the compounds of series **1**, derivative **1Cl** and **1NO$_3$** display the most hypsochromically shifted spectra with a highly structured profile closely resembling the corresponding low-temperature emission. Moving to **1BF$_4$**, **1PF$_6$**, **1OTf** and **1BPh$_4$** the

corresponding emission maximum shows a bathochromic shift that is accompanied by a partial loss of the vibronic structure, indicative of an energetic stabilization of the emitting excited state and an increased degree of CT mixing of the latter. Remarkably, all the compounds of series **1** display intense emission in the solid-state with PLQY in the range 0.07–0.39, being the highest value within the set of derivatives recorded for compound **1Cl**. Interestingly, this high value of PLQY in condensed phase may point toward the fact that triplet-triplet annihilation (TTA) phenomena are not very efficient in the solid state for this class of emitters despite their very long-lived excited states (*vide infra*).

The nature of the diphosphine plays a role as well in modulating the emission in the solid state as shown in Figure 5. The maximum of the emission spectra varies from 484 nm to 580 nm, being the most hypsochromically shifted spectrum observed for compound **6**. Given the rather similar electronic effect exerted by the various diphosphines investigated, the observed spectral changes should be mainly ascribed to change of the local environment due to slightly different arrangements of the luminescent metal complexes in the solid state. Nevertheless, excited state lifetimes are comparable instead with values in the range 93.3–148.3 μs, clearly indicating the similar nature of the emissive excited state within the series of complexes. Compound **5** shows the emission profile peaking at the longest wavelength value of the series. PLQY are lower than the archetypal derivative **1PF$_6$** and shows moderate values falling in the range 0.06–0.13. It is interesting to notice that those values are slightly higher than the corresponding phenylpyridine-based derivatives **6**–**7**.

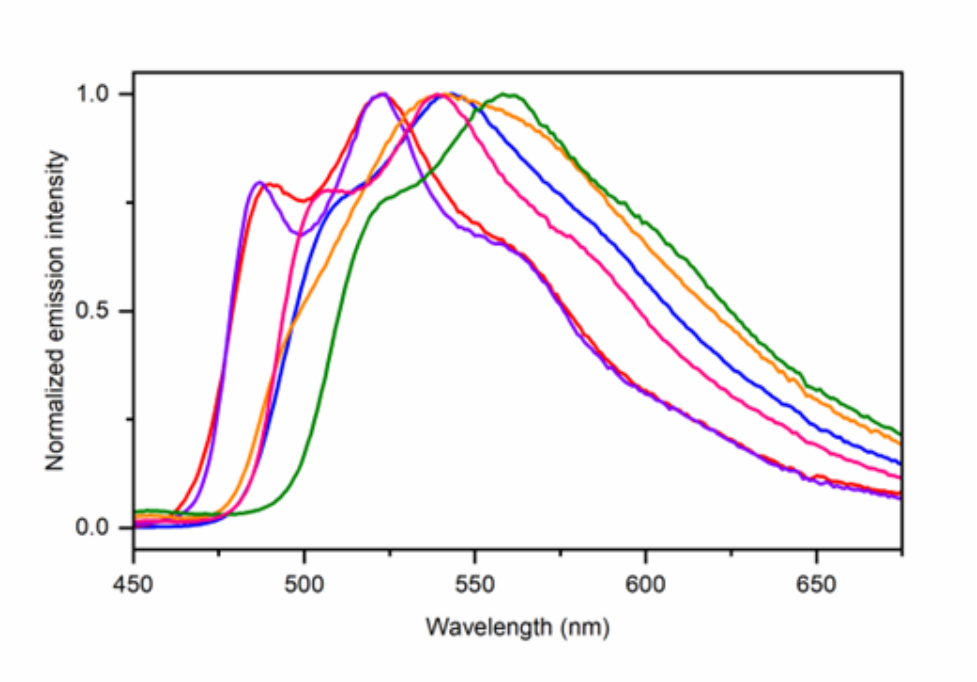

Figure 4. Emission spectra in the solid state of compounds of series **1** upon excitation at at λ_{exc} = 360 nm. Compounds **1PF$_6$** (blue), **1Cl** (red), **1NO$_3$** (violet), **1OTf** (orange), **1BPh$_4$** (dark green), and **1BF$_4$** (magenta).

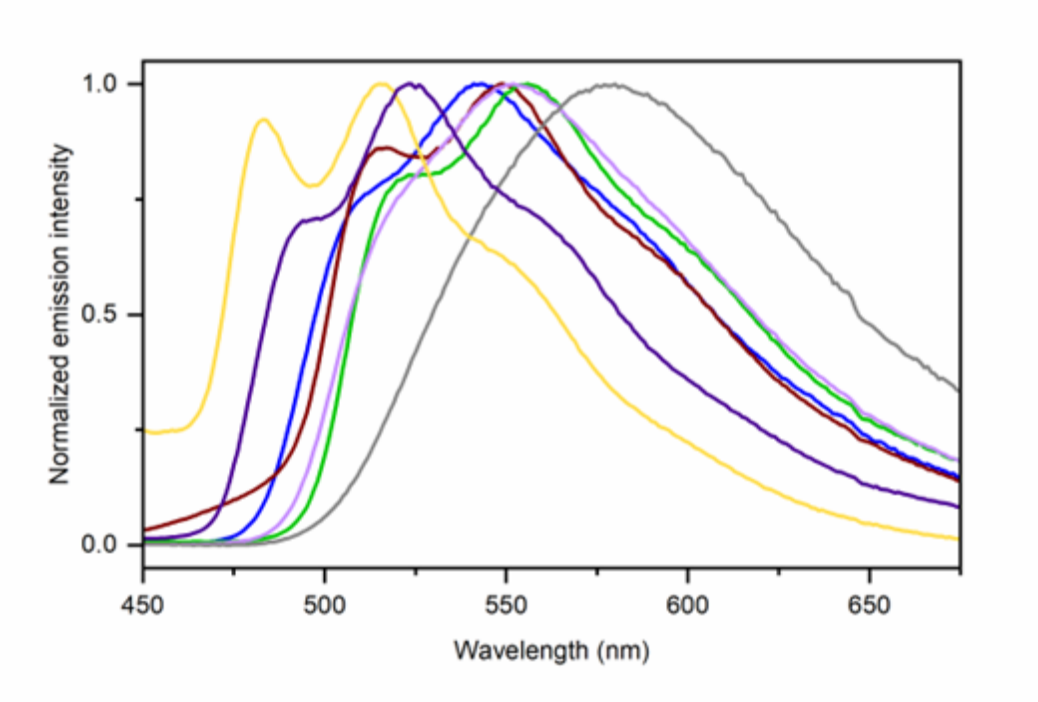

Figure 5. Emission spectra in the solid state of compounds **1PF$_6$** (blue), **2** (brown), **3** (green), **4** (lilac), **6** (yellow) and **7** (purple) upon excitation at λ_{exc} = 360 nm. Compound **5** (grey) was excited at λ_{exc} = 420 nm.

For all the investigated derivatives, the structured emission spectra observed in the solid state closely resemble those recorded at low temperature, pointing towards an excited state with mainly ^{3}LC characters with some degree of admixing with the close-lying CT states involving the biphenyl C^C ligand. Analysis of the crystallographic arrangement (see above) rules out the establishment of any Au(III)···Au(III) short contacts or extended π-π stacking that might give rise to broader, lower-energy, bands with either metal-metal to ligand charge transfer (MMLCT) or excimeric character. Although the formation of the former is debated in spite of short Au(III)···Au(III) contacts is in some cases observed,[52] a few studies reports on this latter possibility.[45,53,54]

Table 2. Photophysical properties of complexes **1**–**7** in dilute CH_3CN solution at room temperature in air-equilibrated condition and at 77 K in 2-MeTHF frozen matrix.

	λ_{max} (ε)	λ_{em}	τ_{obs}	$\bar{\tau}_{obs}$
compound	[nm, (10^3 M^{-1} cm^{-1})]	[nm]	[µs]	[µs]
	room temperature		*77 K*	
1PF$_6$	262 *sh* (52.5), 318 (5.0)	490, 530, 571	111.9 (54%) 168.1 (46%)	143.4
1Cl	261 *sh* (47.5), 317 (4.5)	492, 530, 570	157.5 (47%) 99.2 (53%)	133.3
1NO$_3$	209 *sh* (133.6), 243 (73.5), 258 (62.4), 316 (7.4)	492, 529, 567	143.6 (81%) 73.1 (19%)	139.9

1OTf	241 *sh* (77.6), 259 *sh* (62.9), 317 (7.0)	489, 525, 567	117.9 (54%) 170.4 (46%)	146.9
1BPh$_4$	239 *sh* (85.1), 258 *sh* (63.2), 318 (5.0)	490, 527, 569	101.9 (44%) 161.8 (56%)	148.4
1BF$_4$	208 (119.7), 243 (71.8), 260 *sh* (60.2), 317 (5.6)	491, 527, 570	110.4 (53%) 170.3 (47%)	145.0
2	254 (67.9), 318 (3.9)	489, 524, 568	143.7 (47%) 83.6 (53%)	119.9
3	247 (61.3), 318 (5.1)	494, 533, 575	100.2 (38%) 150.8 (62%)	136.2
4	247 (60.6), 316 (4.8)	496, 534, 575	160 (43%) 92.0 (57%)	130.6
5	250 *sh* (56.7), 315 (4.6)	500, 533, 570	54.5 (65%) 124.7 (35%)	93.3
6	224 *sh* (55.1), 265 (12.3), 305 (8.0)	480, 508, 546	18.0 (84%) 51.4 (16%)	29.8
7	221 *sh* (62.8), 269 (32.2)	476, 512, 551	67.07	-

sh denotes a shoulder.

Table 3. Photophysical properties of complexes **1**–**7** in the solid state at room temperature.

compounds	λ_{em} [nm]	PLQY	CIE (x,y)		τ_{obs} [µs]	$\bar{\tau}_{obs}$ [µs]	k_r [10^4 s^{-1}]	k_{nr} [10^4 s^{-1}]
1PF$_6$	510, 543	16%	0.36	0.55	5.2 (19%) 0.9 (81%)	3.4	4.6	24.4
1Cl	490, 523, 560	39%	0.29	0.54	39.5 (17%) 87.1 (83%)	83.0	0.47	0.73
1NO$_3$	487, 524, 565	18%	0.30	0.51	51.2 (68%) 22.0 (32%)	49.2	0.36	1.7
1OTf	497, 540	7%	0.33	0.43	17.5		0.39	5.3
1BPh$_4$	523, 558	13%	0.39	0.50	36.7		0.35	2.4
1BF$_4$	505, 539, 578	11%	0.33	0.50	15.8 (31%) 45.0 (69%)	41.0	0.26	2.2
2	516, 550, 590	6%	0.30	0.40	9.9 (65%) 3.0 (32%)	8.9	0.67	10.4
3	524, 556, 602	11%	0.38	0.50	40.0 (78%) 15.4 (22%)	37.6	0.29	2.4

4	519, 552	13%	0.37	0.48	35.4	-	0.36	2.4
5	570	11%	0.40	0.43	22.6	-	0.49	3.9
6	484, 517, 551	5%	0.23	0.30	22.1 (30%) 9.7 (42%) 1.4 (28%)	16.8	0.29	5.6
7	495, 523, 560	2%	0.24	0.30	0.6 (51%) 2.2 (49%)	1.8	1.1	52.7

The bulkiness of both biphenyl C^C and chelating P^P ligands that feature two *tert*-butyl and diphenyl-based phosphines, respectively, effectively helps to suppress emitters aggregation and to avoid significant spectral broadening in condensed phase. Time-resolved analysis of the photoluminescence helps to shed a better light onto the nature of the emissive excited state (see Table 3 for data). Deactivation kinetics show (average) lifetime in the order of 3.4–49.2 μs, clearly indicating a sizeable triplet nature of the emitting excited state. No detectable rise time is present, ruling out any excimer emission. A shorter lifetime is observed for Pt(II) derivative **7**, expectantly, indicating that likely a more efficient spin-orbit coupling (SOC) process for this latter compound. Indeed, the very long-lived excited state corroborates the idea that single-triplet mixing via SOC is inefficient in these biphenyl-Au(III) complexes. This is the consequence of the highly stabilized d orbitals of the Au(III) that do not mix efficiently with the π-system of the conjugated chromophore. Hence, the metal atom helps to perturbate the excited state character, but only minor

contribution is expected to the overall orbital composition of the low-lying excited state. This picture is further corroborated by the analysis of the kinetic constant characterizing the emissive excited state. Radiative (k_r) and non-radiative (k_{nr}) rate constants can be estimated from lifetime and PLQY values by using the following equations (eqns. 1–2):

$$k_r = \text{PLQY} / \tau \qquad \text{(eqn. 1)}$$

$$k_{nr} = (1 - \text{PLQY}) / \tau \qquad \text{(eqn. 2)}$$

providing for all the derivatives similar k_r values in the order of 0.26–4.9x10^4 s^{-1}, characteristic of a moderately allowed radiative process. Hence, excited state deactivation processes are largely dominated by radiationless pathways, with the exception of compounds of series **1** that display better emission properties within the whole set of investigated molecules.

Thermal analysis

Thermal stability is an important parameter for evaluating the suitability of organometallic compounds in view of their application in light-emitting devices. To evaluate the thermal properties of these class of emitters, melting point determination and thermogravimetric analyses were carried out and the corresponding thermograms are displayed in Figure S9–S12 of the ESI. All the analysed biphenyl-based compounds possess melting point >250°C, much higher than that recorded for the ppy-Au(III) analogue compound **6** and in the same order of that of the Pt(II) counterpart **7**. Interestingly, thermograms show a wide thermal stability range with 5% weight loss temperature ($T_{5\%}$) well above 200°C for all the investigated derivatives. Overall, these finding

confirm the superior thermal stability of this class of organometallic emitters and prompted their further use in light-emitting optoelectronic devices.

Electrochemical characterization

The electrochemical properties of complexes **1PF$_6$**, **3**, **6** and **7** were assessed by cyclic voltammetry (CV) recorded in acetonitrile with 0.1 M of tetra *n*-butylammonium tetrafluoroborate at room temperature and are referred to saturated calomel electrode (SCE). Data are reported in Table 4 and Figure S13 of the ESI. Both (C^C)-based complexes **1PF$_6$** and **3** show a similar electrochemical behaviour with an irreversible cathodic wave peaking at –1.42 and –1.53 V, respectively. The platinum(II) complex **7** shows a reversible cathodic process peaking at –1.65 V at a similar potential than its [(C^C)Au]-based analogue **3**. The dicationic (C^N)-based gold(III) complex **6** shows a different electrochemical behaviour with a reversible cathodic peak at +0.17 V and two irreversible peaks at –1.61 and –1.73 V respectively.

Table 4: Reduction peaks for complexes **1PF$_6$**, **3**, **6** and **7** in MeCN with 0.1 M $TBABF_4$ *vs* SCE.

Complex	E_{pc} (V)
1PF$_6$	–1.42 (irreversible)
3	–1.53 (irreversible)
6	+0.17 (reversible); –1.61 (irreversible); –1.73 (irreversible)
7	–1.65 (reversible)

Computational investigation

The structures of complexes $\mathbf{1}^+$, $\mathbf{2}^+$, $\mathbf{3}^+$, $\mathbf{4}^+$, $\mathbf{5}^+$, $\mathbf{6}^+$ and $\mathbf{7}^+$ were optimized by mean of DFT in CH_3CN as the solvent. The computed geometric parameters (Table S2–S8 of the ESI) agree well with the experimental data (Table 1). We present in Figure 6 the frontier orbitals of $\mathbf{3}^+$, as an example of this series of complexes. The highest-occupied molecular orbital (HOMO) is located on the biphenyl ligand and is an orbital with a pure π character. On the other hand, the lowest unoccupied molecular orbital (LUMO) has a σ antibonding nature (dσ*) localized between the gold atom and the four coordinated atoms of the ligand with a minor contribution of the phosphine phenyl rings. On the contrary, the LUMO+1 is a π bonding orbital involving the gold and the two ligands with contribution of the π system of the biphenyl scaffold and very small contribution of the phenyl rings of the P^P moiety. The nature of the FMOs in $\mathbf{6}^+$ are rather similar in nature as those computed for derivative $\mathbf{3}^+$ (Figure S14), but the LUMO of the former compound is much lower in energy than that of the latter (Table S8). In $\mathbf{7}^+$, the HOMO is still mainly located on the phenylpyrdine ligand but with some contribution from the metal (Figure S14), however the nature of the LUMO is rather different compared to the series of Au(III) complexes, being now also located on the phenylpyrdine ligand with contribution from the platinum atom. This change in the LUMO nature of $\mathbf{7}^+$ is reflected into the different behaviour towards reduction observed via electrochemistry (see Table 4). The presence of a phenyl ring in $\mathbf{1}^+$ as a linker between the two phosphorus atoms slightly modifies this picture (Figure S15). This phenyl ring contributes to both LUMO and LUMO+1. The HOMO remains purely localized on the biphenyl in $\mathbf{1}^+$. For all the complexes, the HOMO-LUMO gap is in good agreement with the estimated E(0,0) value calculated using the maximum of absorption at the longer wavelength flank (Table S8).

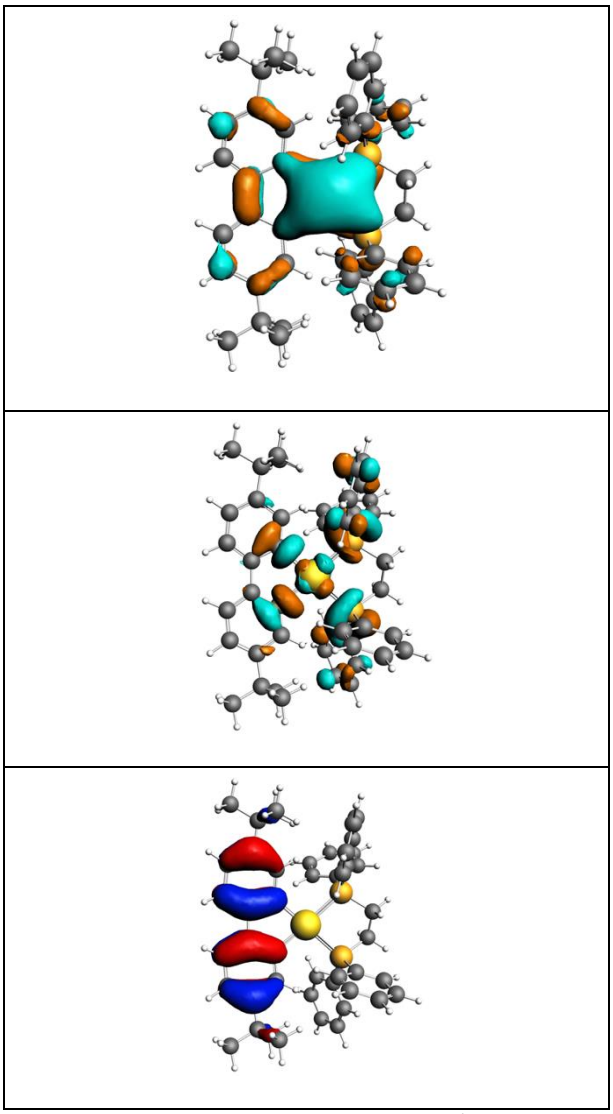

Figure 6. Isodensity surface plot of the FMOs of complex $\mathbf{3}^{+}$: HOMO (*bottom*), LUMO (*middle*) and LUMO+1 (*top*).

The computed absorption spectra are reported in Figure 7. The computed spectra of $\mathbf{1}^+$ exhibits a shoulder around 300 nm and an intense peak centred at 260 nm in good agreement with experimental data (Table 2, λ_{abs} = 262 and 318 nm for complex **1PF$_6$**, for example). A very weak absorption band is also present at 409 nm. This band is generated by the first computed singlet for $\mathbf{1}^+$ (**1**S_1, Figure 8), which is a transition with intraligand character localized on the biphenyl ($^1IL_{CC}$) (CC = biphenyl) admixed with a charge transfer process from the biphenyl towards the gold ($^1L_{CC}MCT$) and from the biphenyl to the diphosphine ligand ($^1L_{CC}L_{PP}CT$), where PP = diphosphine.

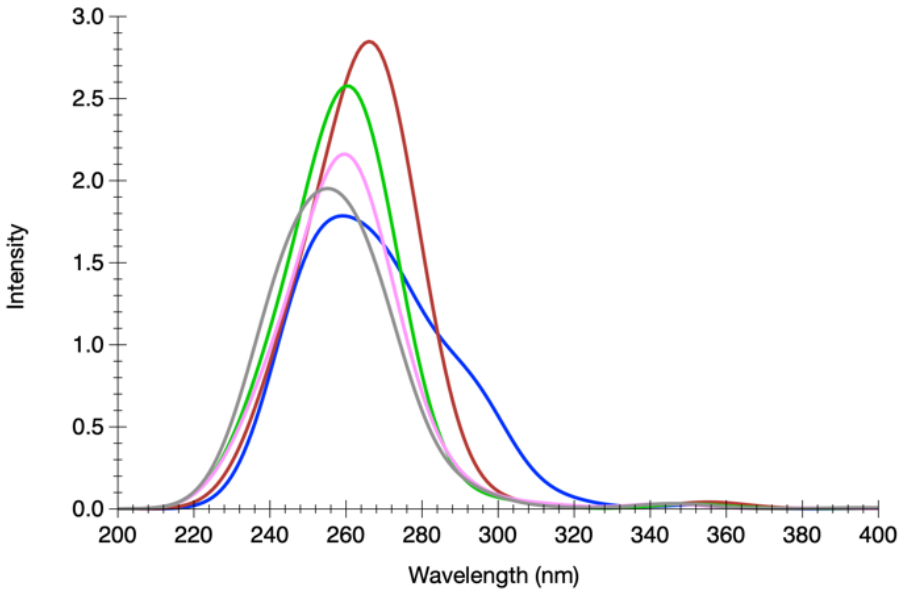

Figure 7. Computed absorption spectra of $\mathbf{1}^+$ (blue), $\mathbf{2}^+$ (brown), $\mathbf{3}^+$ (green), $\mathbf{4}^+$ (lilac), and $\mathbf{5}^+$ (grey) in acetonitrile.

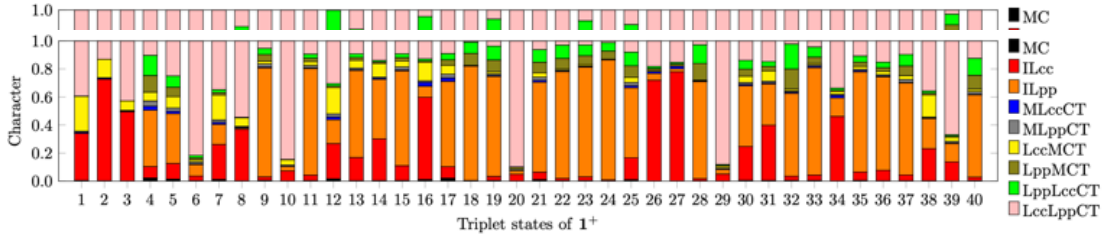

Figure 8. Nature of the computed singlet (*top*) and triplet (*bottom*) states at Franck-Condon (FC) geometry of $\mathbf{1}^+$. Subscript CC and PP stands for the biphenyl ligand and diphosphine ligand, respectively.

The computed intense band at 260 and 300 nm is the result of the contribution of several electronic transitions (Table S9 of the ESI). The shoulder around 300 nm is mainly due to the eighth singlet state ($\mathbf{1}S_8$), which has a largely mixed nature with a major contribution from $^1IL_{PP}$. The band at higher energy (260 nm) is generated by several singlet states, the most important being $\mathbf{1}S_{13}$, $\mathbf{1}S_{15}$, $\mathbf{1}S_{16}$, $\mathbf{1}S_{17}$, $\mathbf{1}S_{22}$, $\mathbf{1}S_{26}$, $\mathbf{1}S_{28}$, $\mathbf{1}S_{31}$, $\mathbf{1}S_{34}$, $\mathbf{1}S_{36}$ and $\mathbf{1}S_{40}$. All these electronic transitions have similar oscillator strength (Table S9) and are mainly IL_{PP} and $L_{CC}L_{PP}CT$ with minor $L_{PP}L_{CC}CT$, $ML_{PP}CT$ and L_{CC} contributions.

The absorption spectra of complexes $\mathbf{2}^+$, $\mathbf{3}^+$, $\mathbf{4}^+$ and $\mathbf{5}^+$ are similar both in nature and energy to that of $\mathbf{1}^+$ (Figure 7 and Table S10–S13). Especially the nature of the frontier molecular orbitals (FMOs) is similar for all complexes (Figure 6).

To gain deeper insights into the luminescence properties of the investigated complexes the lowest triplet state (T_1) of the different structures were optimized. The potential energy surface (PES) of the state T_1 exhibits several local minima. A first optimization leads to a structure (T_1a) originating from the HOMO–LUMO transition (Figures S16 and S17 of the ESI). This implies the population of the dσ* orbital between the metal and both ligands. Upon geometry optimisation, distortion of the coordination sphere around the gold atom from a roughly square-planar to a flattened tetrahedral environment is observed. This can be illustrated by the increase of the C–C–P–P dihedral angle from 1.4° in the ground state of $\mathbf{1}^+$ to 22.0° in the T_1a geometry (Table 5). Similar trend is observed in the other complexes.

A second minima of the T_1 PES, namely T_1b, corresponds to a highly distorted structure. In T_1b, the complexes adopt a *cis*-divacant arrangement (Figure S18). This state has a very mixed nature (see Figure 9) with some degree of metal centred (MC) character.

For $\mathbf{1}^+$, a third minimum of the T_1 PES (T_1c) is obtained and can be described as roughly issued from the HOMO to LUMO+1 excitation. This state corresponds to the T_2 at ground state geometry. Upon geometry optimization, the overall shape of the complex remains the same as illustrated by the ∠C–C–P–P dihedral angle of –0.1°.

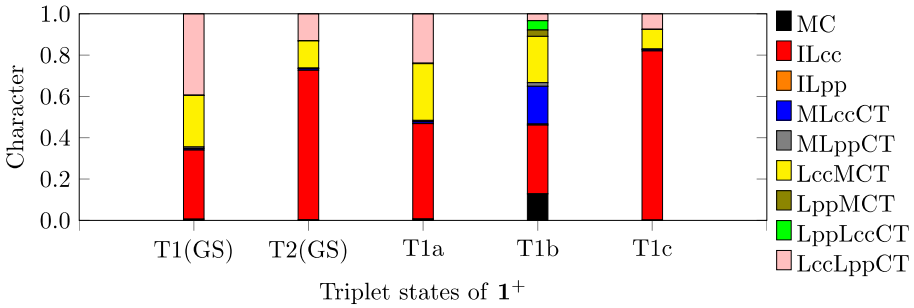

Figure 9. Nature of the T_1 and T_2 states at Franck-Condon geometry of $\mathbf{1}^+$, namely T_1(GS) and T_2(GS), and of T_1a, T_1b and T_1c at their optimized geometry. Subscript CC and PP stands for the biphenyl ligand and diphosphine ligand, respectively.

In complex $\mathbf{1}^+$, the most stable minimum of the T_1 PES corresponds to the structure of T_1b according to the E_{stab} energies (see Figure S16 in ESI for details on definition). The associated emission wavelength computed at 4733 nm is far in the IR domain, corresponding to a quenching state in agreement with the experimental data in solution. The lowest emissive state is T_1a, which emits at 639 nm in solution, also deviates from the experimental values recorded in solid state at 510 and 543 nm (Table 3). The origin of such discrepancy can have a two-fold origin. On one hand, the above values are computed in solution whereas the experimental emission are recorded in solid state. On the other hand, the nuclear flexibility associated to T_1a has been neglected so far.

Indeed, the evolution of the coordination sphere due to the out-of-plane distortion generates two formally degenerate minima (Figure S17) associated to a positive and negative value of the C–C–P–P dihedral angle. Using GAUSSIAN, we were able to locate the transition state separating the two conformers of T_1a of $\mathbf{1}^+$. The energetic barrier has $\Delta G^{\ddagger}$ as small as 2.7 kcal/mol, which is negligible at room temperature. Nevertheless, at this stage we cannot conclude whether an ultrafast hopping process between these two isoenergetic localized minima or a delocalization between these two triplet states takes place. In both cases, computed wavelengths are in reasonable agreement with the experimental value recorded in the solid state. This point requires further investigation, but it is out of the scope of the present manuscript.

Table 5. Energetic and structural parameters computed for complex $\mathbf{1}^+$. Energetic and structural parameters calculated for ground and different triplet exited state geometries. Distortion (E_{dist}), emission (E_{em}) and stabilisation energies (E_{stab}) are given in eV. Emission wavelength (λ_{em}) is given in nm. Distances are expressed in Å and dihedral angles in [°]. [a)] GAUSSIAN calculations; [b)] structure of the transition state.

	GS	**T_1a**	**T_1b**	**T_1c**	**T_1a[a]**	**T_1a[a,b]**
E_{dist}		0.481	2.019	0.338	0.493	0.378
E_{em}		1.941	0.262	2.273	1.957	2.187
E_{stab}		2.422	2.281	2.610	2.450	2.565
λ_{em}		639	4733	545	634	567
Au–C	2.086	2.136	2.307	2.066	2.124	2.071
Au–C	2.087	2.114	2.100	2.067	2.140	2.071
Au–P	2.425	2.474	2.405	2.423	2.459	2.431
Au–P	2.432	2.428	2.502	2.418	2.494	2.431
C_b–C_b	1.463	1.424	1.471	1.384	1.426	1.384
∠C–C–P–P	1.4	22.0	71.7	-0.1	-21.3	0.0

The PES of T_1 for the complexes $\mathbf{2}^+$, $\mathbf{3}^+$, $\mathbf{4}^+$ and $\mathbf{5}^+$ present a T_1a state similar to that of $\mathbf{1}^+$, associated to an out-of-plane dihedral angle ranging from 15 to 30° (see Table S2–S7). As for $\mathbf{1}^+$, several conformational minima are associated to T_1a connected by almost planar transition state. That computed for $\mathbf{3}^+$**,** following the same method as for $\mathbf{1}^+$**,** leads to a barrier of 4.0 kcal/mol. For all these complexes, a T_1b minimum lower in energy than T_1a, was also found, which is most likely responsible of the emission quenching in solution. Finally, another minimum (T_1d) was found for $\mathbf{2}^+$, which is a conformer of T_1a. The nature of the state is the similar, but one of the Au–P bonds is broken with a distance of 3.743 Å (see Supplementary Information).

The anion effect observed on series **1** complexes was explored as well. The same study as for $\mathbf{1}^+$ was performed on the complex **1Cl** with an explicit chloride anion included in the calculation. The effect on the absorption spectra is small and especially the nature of the frontier orbitals remain the same as in $\mathbf{1}^+$ (Figure S15). However, the optimization of the potentially emitting states T_1a and T_1c put in evidence a significant effect on the luminescence properties. Especially in **1Cl**, the emission wavelength of T_1a display a sizeable hypsochromic shift, being computed at 557 nm (vs. 639 nm for T_1a in $\mathbf{1}^+$). This shift is associated to a reduction of the C–C–P–P out-of-plane distortion which is reduced to –10.6° in **1Cl** compared to 22.0° in $\mathbf{1}^+$. This highlights the crucial role played by the out-of-plane distortion in the emission properties of the investigated series of complexes and the origin of the anion effect which is due to its influence on this distortion.

From all these data, we can rationalise the experimental emission properties as follows. In solution, the complexes are not luminescent since excitation energy is funnelled into the lowest-energy quenching structure T_1b, which is computed to emit in the IR domain. Hence, strong non-radiative vibronic coupling is expected between this state and the ground state. However, the presence of free coordination sites in the coordination sphere, which corresponds to a *cis*-divacant

octahedron, paves the way for further radiationless mechanisms, such as complex-solvent exciplex formation, solvent coordination and ligand de-coordination. This latter case would be most likely associated to the neutral diphosphine de-coordination.

In solid state, such detrimental and large structural changes are prevented by the crystal packing effect and rigidification of the environment, thus the emission properties of the complexes are restored. After relaxation of the excited state, the square-planar arrangement around the $5d^8$ Au(III) centre becomes highly distorted due to the population of the anti-bonding dσ* Au–L orbital (HOMO, Figure 6). This population leads to a flattened tetrahedral structure as shown by the values computed for the C–C–P–P dihedral angle and generates two minima connected by a transition state. The computed values for the energetic barrier are rather small and the computed emission wavelength fairly agrees with the experimental values. This is further supported by the calculation effect on **1Cl** complex compared to the free cation $\mathbf{1}^+$. We observe a strong blue shift of the emission wavelength associated to a reduction of the out-of-plane distortion. This suggests that the anion effect is not due to a change in the state nature, but to constraints imposed on the structure distortion. Furthermore, we propose that the difference observed between the complexes excited state lifetime is linked to interconversion barrier between the minima and the value of the C–C–P–P angle. Furthermore, the state T_1c being close to T_1a can contribute to the emission. Finally, we attribute the loss of emission of complex $\mathbf{2}^+$ to the presence of the T_1d minimum that leads to a partial de-coordination of the phosphine ligand.

Electroluminescent characteristics of LECs

The LECs employing complexes **1PF$_6$** and **3** were fabricated and measured to test their EL properties. The EL characteristics of these LECs are summarized in Table 6. The EL spectra of the

LECs based on complexes **1PF$_6$** and **3** with various emissive-layer thicknesses are shown in Figure 10a and 10b, respectively. To realize better device performance, constant currents and constant voltages were employed for measuring the LECs based on complexes **1PF$_6$** and **3**, respectively. For each LEC with certain device thickness, the current or voltage was chosen to achieve the best device efficiency. Since complexes **1PF$_6$** and **3** possess similar molecular structures, the LECs employing both complexes exhibited similar yellow EL spectra. In addition, the EL spectra of LECs resemble the PL spectra of their emissive layers. It confirms that similar mechanisms are responsible for both EL and PL emission. However, the EL spectra of the LECs with thicker emissive layers showed EL spectra deviated from the PL spectra slightly. It can be attributed to the modified microcavity effect induced by the adjusted device optical structure.[55–57]

The time-dependent voltage, brightness, and EQE of the LECs based on complex **1PF$_6$** with various emissive-layer thicknesses are depicted in Figure 11a, 11b, and 11c, respectively. When the LEC was operated under a constant current, the device voltage was initially high because of the high carrier injection barrier into the undoped emissive layer. With the gradually established electrochemically doped layers, the device voltage then decreased due to the subsequently reduced carrier injection barrier. When reaching a steady state, a lower voltage was required to maintain a lower device current. Since the initial voltage was high to enforce the target current to be injected into the device, the brightness increased rapidly after the current was applied owing to improved carrier balance. The brightness then decreased with time gradually due to the material degradation and/or the exciton quenching by the extending doped layers.[58] Under a constant current, the EQE followed the same temporal evolution trend as brightness. The peak EQE reached *ca.* 1% for the LEC based on complex **1PF$_6$** with the optimized emissive-layer thickness (158 nm). These data

reveal that moderate device efficiency can be obtained from the LECs based on the proposed ionic gold complex **1PF$_6$**.

Table 6. Summary of the EL characteristics of the LECs based on complexes **1PF$_6$** and **3**.

Complex	Concentration (mg mL^{-1}) [a]	Thickness (nm)	Operation condition [b]	EL_{max} (nm) [c]	CIE 1931 (x, y)	B_{max} (cd m^{-2}) [d]	$\eta_{ext, max}$ (%) [e]	$\eta_{P, max}$ (cd A^{-1}) [f]	$\eta_{P, max}$ (lm W^{-1}) [g]
1PF$_6$	40	100	15 μA	559	(0.43, 0.55)	16.01	0.34	1.07	0.42
	60	158	1 μA	561	(0.45, 0.53)	2.56	0.98	2.56	1.10
	80	236	3 μA	521	(0.37, 0.58)	7.77	0.83	2.59	0.82
3	80	235	10 V	550	(0.41, 0.56)	0.97	0.57	1.77	0.56
	100	289	11 V	570	(0.47, 0.51)	0.64	0.88	2.48	0.71
	120	357	11 V	561	(0.45, 0.52)	0.50	0.68	1.58	0.45

[a] Solution concentration for spin coating at 2000 rpm. [b] Constant current or constant voltage. [c] Stabilized EL emission peak wavelength. [d] Maximal brightness. [e] Maximal external quantum efficiency. [f] Current efficiency. [g] Power efficiency.

On the other hand, the time-dependent current, brightness, and EQE of the LECs based on complex **3** with various emissive-layer thicknesses are shown in Figure 12a, 12b, and 12c, respectively. After a constant bias was applied, the mobile ions in the emissive layer of the LEC drifted toward electrodes and lead to gradually formed electrochemically doped layers, leading to increasing device current with time. However, the device turn-on speed of the LECs employing

complex **3** was lower than that of the LEC based on complex **1PF$_6$** since the 1-butyl-3-methylimidazolium hexafluorophosphate [$BMIM^+(PF_6)^-$] concentration was lower. The brightness and the EQE also increased gradually with device current due to improved carrier balance. After reaching the peak value, the brightness and the EQE decreased with time gradually because of the material degradation and/or the exciton quenching by the doped layers. The peak EQE reached *ca.* 0.9% for the LEC based on complex **3** with the optimized emissive-layer thickness (289 nm). Compared with complex **1PF$_6$**, slightly lower EL efficiency of complex **3** may be attributed to the lack of phenyl ring for steric hindrance. In spite of many reported organic light-emitting diodes (OLEDs) based on neutral Au(I) and Au(III) complexes,[14] the published LECs employing ionic gold complexes are still scarce. To the best of our knowledge, this work demonstrates the first LECs based on ionic gold complexes. It shows the potential of gold complexes for use in LECs and opens a new avenue for this type of materials.

Based on the solid-state PLQYs shown in Table 3 (16% and 11% for complex **1PF$_6$** and **3**, respectively), the EQEs obtained from the LECs based on complex **1PF$_6$** and **3** reached *ca.* 30 and 40%, respectively, of their theoretical maximum values when considering the following equation (eqn. 3) to determine the theoretical device EQE.

$$\eta_{EQE} = \eta_{out} \times \gamma \times \eta_{S,T} \times \eta_{QY} \qquad \text{eqn. 3}$$

In this equation, η_{EQE} is the device EQE, η_{out} is the light outcoupling efficiency, γ is the factor of carrier balance, $\eta_{S,T}$ is the emissive exciton generation efficiency and η_{QY} is the thin-film PLQY. η_{out} is *ca.* 20% for a bottom-emitting device and $\eta_{S,T}$ is 100% for phosphorescent complexes. If the carrier balance is perfect, γ would be 100%. Measured EQEs were lower than the theoretical maximum values due to imperfect carrier balance of the LECs. The degree of carrier balance of the LECs based on complex **1PF$_6$** and **3** (γ = *ca.* 30 and 40%, respectively) was significantly lower

than that (γ >70%) reported for the state-of-the-art LECs employing iridium complexes (EQE >10%).[59,60] However, the device efficiencies of the proposed LECs based on gold complexes were either higher than[61,62] or comparable with[63,64] those of the reported LECs employing copper complexes exhibiting similar emission spectra and PLQYs. Compared with ruthenium complexes, the proposed gold complexes showed comparable EL efficiencies, but the yellow EL emission spectra of gold complexes were beneficial in obtaining higher current efficiencies (cd A^{-1}) and power efficiencies (lm W^{-1}) due to better spectral overlap with the spectral sensitivity of human eyes.[65,66] These comparison results indicate that similar to iTMCs other than the iridium complexes, more sophisticated studies on enhancing the PLQYs of gold complexes and improving the carrier balance of the LECs based on gold complexes would be required for them to reach the device performance of LECs based on iridium complexes.

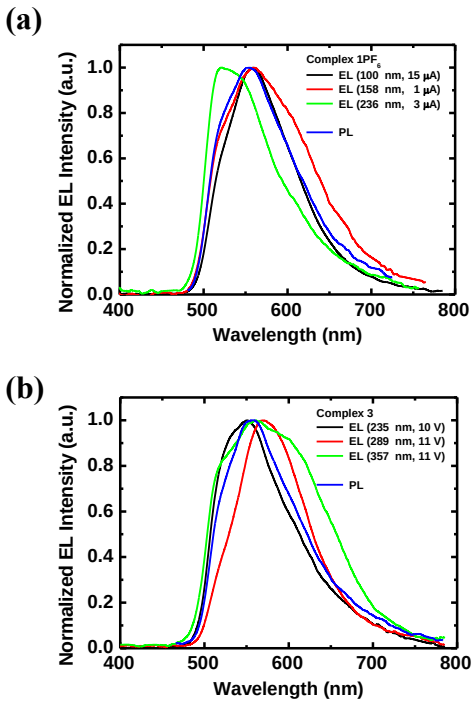

Figure 10. Thickness-dependent EL spectra of the LECs based on complexes (a) **1PF6** and (b) **3**. The device thickness and driving current/voltage of each device are shown in the inset. The PL spectra of the emissive layers are also shown for comparison.

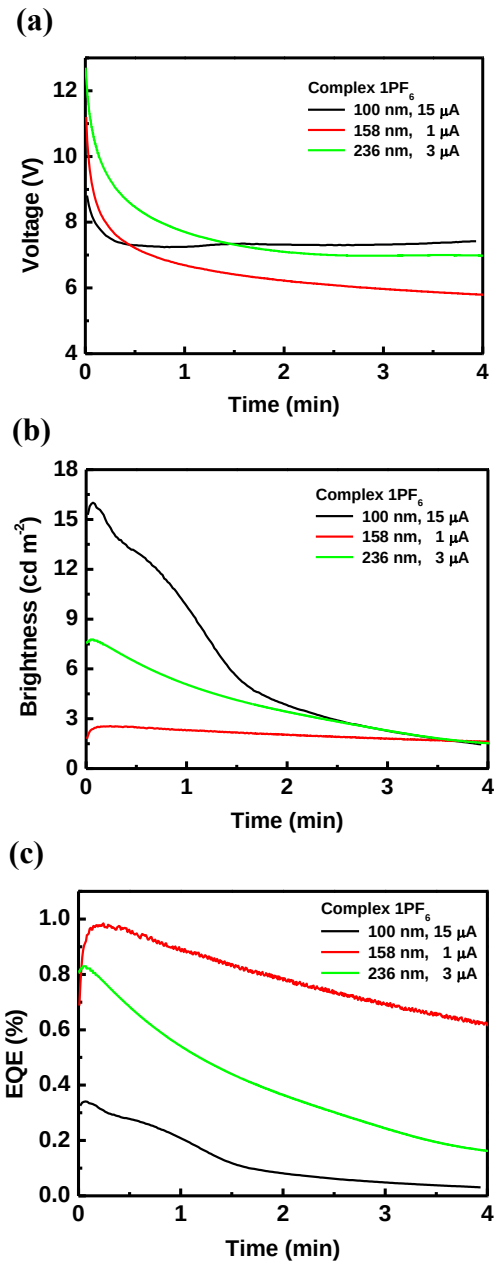

Figure 11. Time-dependent (a) voltage, (b) brightness, and (c) EQE of the LECs based on complex **1PF6**. The device thickness and the driving current of each device are shown in the inset.

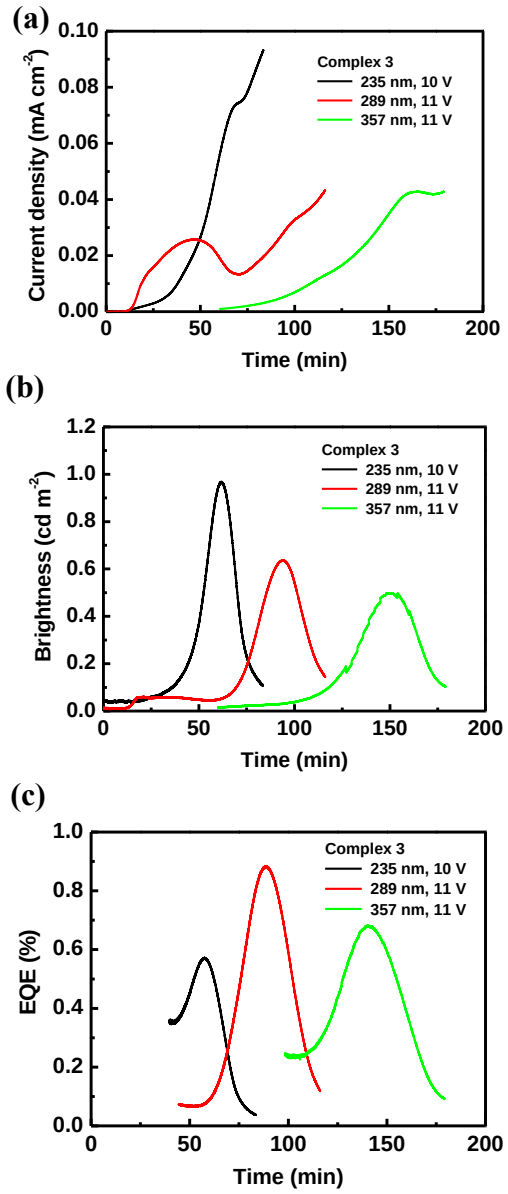

Figure 12. Time-dependent (a) current density, (b) brightness, and (c) EQE of the LECs based on complex **3**. The device thickness and the bias voltage of each device are shown in the inset.

Conclusions

The synthesis of a series of ten novel organometallic gold(III) complexes of general formula [(C^C)Au(P^P)]X is described by varying the nature of the chelating diphosphine ligand and the

counterion. The dicationic [(C^N)Au(P^P)]$(PF_6)_2$ and platinum(II) [(C^N)Pt(P^P)]PF_6 analogues have also been synthesized for comparison purposes. Among these, the single-crystal structure and packing of seven complexes was unambiguously assessed by means of X-ray diffractometric analysis that confirmed the absence of intermolecular interactions, e.g. Au–Au short contacts and/or π-stacking. The complexes appeared to be strongly luminescent in solid state as neat powder samples. The influence of the nature of both the diphosphine ligand and the counteranion was investigated with **1Cl** showing the highest quantum yield (39%). The nature of the emission was ascribed to a ^{3}LC localized on the formally *bis*-anionic C^C ligand as also confirmed by TD-DFT calculations. Due to their favourable thermal and electrochemical stability and strong luminescence properties, complexes **1PF$_6$** and **3** were selected for the fabrication of solution-processed LECs. The device made using **1PF$_6$** displayed a green-yellow electroluminescence with EQE up to 1%. Although the EQE are still moderate, this represents the first report on the use of gold(III) complexes for LEC devices and demonstrated the potential application of such class of emitters as electroluminescent materials devices beyond classical OLEDs, thus opening the way for further developments and improvements.

ASSOCIATED CONTENT

Experimental section

General remarks

Anhydrous solvents were obtained by standard procedures. Chemicals were purchased from various manufacturers and used as received. ^{1}H, ^{13}C, ^{31}P and ^{195}Pt NMR spectra were acquired Bruker 300, 400 or 600 MHz spectrometers. Chemical shifts (δ) are expressed as ppm referenced to the solvent residual signal. Splitting patterns are expressed as follows: s, singlet; d, doublet; t, triplet; m, multiplet. Mass spectrometry was carried out at the Mass Spectrometry Sciences Sorbonne University (MS3U) platform of Sorbonne Université (Paris). Elemental analysis were performed at the Service Chromato-Masse Microanalyse of the Université Paris-Saclay (Châtenay-Malabry, France). Dimeric gold precursor, [(C^N)$AuCl_2$] and [(C^N)Pt(DMSO)Cl] have been synthesized according to reported procedures.[44,67,68] Diphosphine ligands have been purchased at Sigma-Aldrich and used as received.

Synthesis of complex 1Cl

In a Schlenk tube under N_2 atmosphere, the gold dimer (40 mg, 0.04 mmol) is suspended into degassed dichloromethane (4 mL). *Cis*-diphenylphosphinobenzene (36 mg, 0.08 mmol) is added and the reaction is kept under N_2 atmosphere at room temperature for 2 h. The reaction mixture was filtered through a glass frit with Celite and the obtained solution was concentrated under reduced pressure. Upon addition of a large amount of Et_2O, a pale yellow precipitate was formed which was recovered and gave after drying the pure product as a pale yellow powder (69 mg, 0.073 mmol, 91% yield). ^{1}H NMR ($CDCl_3$, 300 MHz, 300 K): δ 7.87 (m, 2 H, H^{13}), 7.60-7.66 (m, 8 H, H^{9}), 7.39-7.54 (m, 18 H, H^{2} + H^{5} + H^{8} + H^{10} + H^{12}), 7.14 (d, $^{3}J_{H-H}$= 8.0 Hz, 2 H, H^{4}), 0.80 (s, 18 H ^{t}Bu). $^{13}C\{^{1}H\}$ Jmod NMR ($CDCl_3$, 75.5 MHz, 300 K): δ 163.1 (dd, $^{2}J_{P-C}$ = 114.1 Hz, $^{2}J_{P-C}$ = 7.9 Hz, C^{6}), 151.7 (s, C^{1}), 150.6 (t, $^{4}J_{P-C}$ = 5.9 Hz, C^{3}), 137.8 (d, $^{1}J_{P-C}$ = 59.8 Hz, C^{11}), 137.5 (d, $^{1}J_{P-C}$ = 59.8 Hz, C^{11}), 135.9 (m, C^{12}), 135.0 (m, C^{13}), 134.8 (t, $^{3}J_{P-C}$ = 8.1 Hz, C^{2}), 134.4 (m, C^{8}), 133.2

(s, C^{10}), 130.2 (m, C^9), 125.0 (s, C^4), 124.6 (d, $^1J_{P\text{-}C}$ = 51.8 Hz, C^7), 122.9 (m, C^5), 34.6 (s, $C_{quat.tBu}$), 30.9 (s, $CH_{3\text{-}tBu}$). $^{31}P\{^1H\}$ NMR ($CDCl_3$, 121.5 MHz): δ 52,4 (s, 2 P, P-Au). ESI-MS (MeCN) *positive mode exact mass for* $[C_{50}H_{48}P_2Au]^+$ (907.2891): measured *m/z* 907.2892 $[M\text{-}Cl]^+$. Calcd for $C_{50}H_{48}P_2AuCl.5H_2O$ (1033.37): C, 58.12; H, 5.66. Found: C, 58.58; H 4.20.

Synthesis of complex 1NO₃

In a Schlenk tube under N_2 atmosphere, the gold dimer (40 mg, 0.04 mmol) is suspended into degassed dichloromethane (4 mL). *Cis*-diphenylphosphinobenzene (36 mg, 0.08 mmol) is added and the reaction is kept under N_2 atmosphere at room temperature for 2 h. Silver nitrate (14 mg, 0.08 mmol) was dissolved into acetonitrile (1 mL) and was then added on the mixture. The reaction was kept at room temperature for another 2 h. The reaction mixture was filtered through a glass frit with Celite and the obtained solution was concentrated under reduced pressure. Upon addition of a large amount of Et_2O, an off-white precipitate was formed which was recovered and gave after drying the pure product as white powder (72 mg, 0.074 mmol, 93% yield). ^1H NMR ($CDCl_3$, 400 MHz, 300 K): δ 7.91 (m, 2 H, H^{13}), 7.54-7.60 (m, 12 H, H^9 + H^{10}), 7.40-7.50 (m, 14 H, H^2 + H^5 + H^8 + H^{12}), 7.18 (d, $^3J_{H\text{-}H}$= 8.0 Hz, 2 H, H^4), 0.81 (s, 18 H ^{t}Bu). $^{13}C\{^1H\}$ Jmod NMR ($CDCl_3$, 100.6 MHz, 300 K): δ 163.1 (dd, $^2J_{P\text{-}C}$ = 112.7 Hz, $^2J_{P\text{-}C}$ = 7.7 Hz, C^6), 151.7 (s, C^1), 151.0 (t, $^4J_{P\text{-}C}$ = 5.9 Hz, C^3), 137.1 (d, $^1J_{P\text{-}C}$ = 59.8 Hz, C^{11}), 136.8 (d, $^1J_{P\text{-}C}$ = 59.8 Hz, C^{11}), 136.2 (t, $^2J_{P\text{-}C}$ = 7.5 Hz, C^{12}), 135.4 (m, C^{13}), 134.9 (t, $^3J_{P\text{-}C}$ = 8.1 Hz, C^2), 134.0 (m, C^8), 133.6 (s, C^{10}), 130.4 (m, C^9), 125.5 (s, C^4), 123.8 (d, $^1J_{P\text{-}C}$ = 51.8 Hz, C^7), 122.1 (m, C^5), 34.6 (s, $C_{quat.tBu}$), 30.9 (s, $CH_{3\text{-}tBu}$). $^{31}P\{^1H\}$ NMR ($CDCl_3$, 121.5 MHz, 300 K): δ 55.4 (s, 2 P, P-Au). ESI-MS (MeCN) *positive mode exact mass for* $[C_{50}H_{48}P_2Au]^+$ (907.2891): measured *m/z* 907.2888 $[M\text{-}NO_3]^+$. Calcd for $C_{50}H_{48}P_2AuNO_3.H_2O$ (987.87): C, 60.79; H, 5.10; N, 1.42. Found: C, 60.45; H 4.81; N, 1.48.

Synthesis of complex 1OTf

In a Schlenk tube under N_2 atmosphere, the gold dimer (40 mg, 0.04 mmol) is suspended into degassed dichloromethane (4 mL). *Cis*-diphenylphosphinobenzene (36 mg, 0.08 mmol) is added and the reaction is kept under N_2 atmosphere at room temperature for 2 h. Silver triflate (20 mg, 0.08 mmol) was dissolved into acetonitrile (1 mL) and was then added on the mixture. The reaction was kept at room temperature for another 2 h. The reaction mixture was filtered through a glass frit with Celite and the obtained solution was concentrated under reduced pressure. Upon addition of a large amount of Et_2O, an off-white precipitate was formed which was recovered and gave after drying the pure product as white powder (66 mg, 0.062 mmol, 77 % yield). ^{1}H NMR ($CDCl_3$, 400 MHz, 300 K): δ 7.88 (s, 2 H, H^{13}), 7.47-7.57 (m, 26 H, $H^2 + H^5 + H^8 + H^9 + H^{10} + H^{12}$), 7.19 (d, $^3J_{H\text{-}H}$ = 8.1 Hz, 2 H, H^4), 0.81 (s, 18 H, ^{t}Bu). $^{13}C\{^1H\}$ Jmod NMR ($CDCl_3$, 100.6 MHz, 300 K): δ 163.4 (dd, $^2J_{P\text{-}C}$ = 113.1 Hz, $^2J_{P\text{-}C}$ = 7.4 Hz, C^6), 151.8 (s, C^1), 151.1 (t, $^4J_{P\text{-}C}$ = 5.9 Hz, C^3), 137.1 (d, $^1J_{P\text{-}C}$ = 60.0 Hz, C^{11}), 136.8 (d, $^1J_{P\text{-}C}$ = 59.0 Hz, C^{11}), 136.2 (t, $^2J_{P\text{-}C}$ = 8.1 Hz, C^{12}), 135.4 (m, C^{13}), 135.0 (t, $^3J_{P\text{-}C}$ = 7.4 Hz, C^2), 134.0 (m, C^8), 133.6 (s, C^{10}), 130.5 (m, C^9), 125.6 (s, C^4), 123.6 (d, $^1J_{P\text{-}C}$ = 54.0 Hz, C^7), 122.1 (m, C^5), 34.7 (s, $C_{quat.tBu}$), 30.9 (s, $CH_{3\text{-}tBu}$). $^{31}P\{^1H\}$ NMR ($CDCl_3$, 121.5 MHz, 300 K): δ 55.4 (s, 2 P, P-Au). ESI-MS (MeCN) *positive mode exact mass for* $[C_{50}H_{48}P_2Au]^+$ (907.2891): measured *m/z* 907.2896 $[M\text{-}OTf]^+$. Calcd for $C_{50}H_{48}P_2AuCF_3SO_3$ (1056.91): C, 57.96; H, 4.58; S, 3.03. Found: C, 58.04; H 4.59; S, 3.06.

Synthesis of complex 1BF$_4$

In a Schlenk tube under N_2 atmosphere, the gold dimer (40 mg, 0.04 mmol) is suspended into degassed dichloromethane (4 mL). *Cis*-diphenylphosphinobenzene (36 mg, 0.08 mmol) is added

and the reaction is kept under N_2 atmosphere at room temperature for 2 h. Sodium tetrafluoroborate (22 mg, 0.2 mmol) was dissolved into acetonitrile (1 mL) and was then added on the mixture. The reaction was kept at room temperature for another 2 h. Dichloromethane (15 mL) is added into the mixture. The reaction mixture was filtered through a glass frit with Celite and the obtained solution was concentrated under reduced pressure. Upon addition of a large amount of Et_2O, an off-white precipitate was formed which was recovered and gave after drying the pure product as white powder (54 mg, 0.054 mmol, 68% yield). ^{1}H NMR ($CDCl_3$, 400 MHz, 300 K): δ 7.88 (broad s, 2 H, H^{12}), 7.40-7.57 (m, 26 H, H^2 + H^5 + H^8 + H^9 + H^{10} + H^{12}), 7.19 (d, $^3J_{H\text{-}H}$ = 8.1 Hz, 2 H, H^4), 0.81 (s, 18 H, ^{t}Bu). $^{13}C\{^1H\}$ Jmod NMR ($CDCl_3$, 75.5 MHz, 300 K): δ 163.3 (dd, $^2J_{P\text{-}C}$ = 112.8 Hz, $^2J_{P\text{-}C}$ = 7.4 Hz, C^6), 151.7 (s, C^1), 151.0 (t, $^4J_{P\text{-}C}$ = 5.9 Hz, C^3), 137.0 (d, $^1J_{P\text{-}C}$ = 59.8 Hz, C^{11}), 136.8 (d, $^1J_{P\text{-}C}$ = 60.3 Hz, C^{11}), 136.1 (t, $^2J_{P\text{-}C}$ = 7.9 Hz, C^{12}), 135.4 (m, C^{13}), 135.0 (t, $^3J_{P\text{-}C}$ = 7.4 Hz, C^2), 134.0 (m, $C^{8/9}$), 133.6 (s, C^{10}), 130.4 (m, $C^{8/9}$), 125.5 (s, C^4), 123.8 (d, $^1J_{P\text{-}C}$ = 54.4 Hz, C^7), 122.0 (m, C^5), 34.6 (s, $C_{quat.tBu}$), 30.8 (s, $CH_{3\text{-}tBu}$). $^{31}P\{^1H\}$ NMR ($CDCl_3$, 121.5 MHz, 300 K): δ 55.5 (s, P-Au). ESI-MS (MeCN) *positive mode exact mass for* $[C_{50}H_{48}P_2Au]^+$ (907.2891): measured *m/z* 907.2904 $[M\text{-}BF_4]^+$. Calcd for $C_{50}H_{48}P_2AuBF_4$ (994.29): C, 60.38; H, 4.86. Found: C, 60.28; H 4.81.

Synthesis of complex 1BPh$_4$

In a Schlenk tube under N_2 atmosphere, the gold dimer (40 mg, 0.04 mmol) is suspended into degassed dichloromethane (4 mL). *Cis*-diphenylphosphinobenzene (36 mg, 0.08 mmol) is added and the reaction is kept under N_2 atmosphere at room temperature for 2 h. Sodium tetraphenylborate (27 mg, 0.08 mmol) was dissolved into acetonitrile (1 mL) and was then added on the mixture. The reaction was kept at room temperature for another 2 h. Dichloromethane (15

mL) is added into the mixture. The reaction mixture was filtered through a glass frit with Celite and the obtained solution was concentrated under reduced pressure. Upon addition of a large amount of Et_2O, an off-white precipitate was formed which was recovered and gave after drying the pure product as white powder (89 mg, 0.073 mmol, 91 % yield). ^{1}H NMR ($CDCl_3$, 400 MHz, 300 K): δ 7.53 (m, 4 H, H^{12} + H^{13}), 7.38-7.47 (m, 30 H, H^5 + H^8 + H^9 + H^{10} + H^{16}), 7.15-7.21 (m, 4 H, H^2 + H^4), 6.95 (t, $^3J_{H\text{-}H}$ = 7.3 Hz, 8 H, H^{15}), 6.81 (t, $^3J_{H\text{-}H}$ = 7.1 Hz, 8 H, H^{17}), 0.82 (s, 18 H, ^{t}Bu). $^{13}C\{^1H\}$ Jmod NMR ($CDCl_3$, 75.5 MHz, 300 K): δ 164.3 (q, $^1J_{B\text{-}C}$ = 49.1 Hz, C^{14}), 163.3 (dd, $^2J_{P\text{-}C}$ = 113.1 Hz, $^2J_{P\text{-}C}$ = 8.1 Hz, C^6), 151.7 (s, C^1), 151.1 (t, $^4J_{P\text{-}C}$ = 6.7 Hz, C^3), 137.0 (d, $^1J_{P\text{-}C}$ = 59.2 Hz, C^{11}), 136.8 (d, $^1J_{P\text{-}C}$ = 59.3 Hz, C^{11}), 136.4 (s, C^{16}) , 135.9 (t, $^2J_{P\text{-}C}$ = 8.1 Hz, C^{12}), 135.3 (m, C^{13}), 134.9 (t, $^3J_{P\text{-}C}$ = 8.1 Hz, C^2), 133.8 (m, $C^{8/9}$), 133.7 (s, C^{10}), 130.5 (m, $C^{8/9}$), 125.6 (s, C^4), 125.5 (q, $^2J_{B\text{-}C}$ = 2.9 Hz, C^{15}), 123.7 (d, $^1J_{P\text{-}C}$ = 53.9 Hz, C^7), 122.2 (m, C^5), 121.6 (s, C^{17}), 34.7 (s, $C_{quat.tBu}$), 30.9 (s, $CH_{3\text{-}tBu}$). $^{31}P\{^1H\}$ NMR ($CDCl_3$, 121.5 MHz, 300 K): δ 55.2 (s, P-Au). ESI-MS (MeCN) *positive mode exact mass for* $[C_{50}H_{48}P_2Au]^+$ (907.2891): measured *m/z* 907.2882 $[M\text{-}BPh_4]^+$. Calcd for $C_{50}H_{48}P_2AuB(C_6H_6)_4.H_2O$ (1245.10): C, 71.39; H, 5.67. Found: C, 71.40; H 5.28.

Synthesis of complexes 1PF$_6$ and 2–5: general method

In a Schlenk tube under N_2 atmosphere, the gold dimer (40 mg, 0.04 mmol) is suspended into degassed dichloromethane (4 mL). The diphosphine (0.08 mmol) is added and the reaction is kept under N_2 atmosphere at room temperature for 2 h. Potassium hexafluorophosphate (37 mg, 0.20 mmol) is dissolved into degasses acetonitrile (1mL) and the reaction is kept under N_2 atmosphere at room temperature for 2h. Some dichloromethane (15 mL) is added into the mixture before filtration. The reaction mixture was filtered through a glass frit with Celite and the obtained

solution was concentrated under reduced pressure. Upon addition of a large amount of Et_2O, a pale yellow precipitate was formed which was recovered and gave after drying the pure product.

Complex 1PF$_6$: *Cis*-diphenylphosphinobenzene (36 mg). The pure product is obtained as a pale yellow powder (63 mg, 0.06 mmol, 75% yield). ^{1}H NMR ($CDCl_3$, 300 MHz, 300 K): δ 7.81 (m, 2 H, H^{13}), 7.44-7.56 (m, 26 H, $H^2 + H^5 + H^8 + H^9 + H^{10} + H^{12}$), 7.19 (d, $^3J_{H\text{-}H}$ = 8.1 Hz, 2 H, H^4), 0.82 (s, 18 H, ^{t}Bu). $^{13}C\{^1H\}$ Jmod NMR ($CDCl_3$, 75.5 MHz, 300 K): δ 163.4 (dd, $^2J_{P\text{-}C}$ = 114.4 Hz, $^2J_{P\text{-}C}$ = 7.9 Hz, C^6), 151.8 (s, C^1), 151.1 (t, $^4J_{P\text{-}C}$ = 5.9 Hz, C^3), 137.0 (d, $^1J_{P\text{-}C}$ = 59.8 Hz, C^{11}), 136.8 (d, $^1J_{P\text{-}C}$ = 59.8 Hz, C^{11}), 136.2 (t, $^2J_{P\text{-}C}$ = 8.3 Hz, C^{12}), 135.5 (m, C^{13}), 135.1 (t, $^3J_{P\text{-}C}$ = 7.8 Hz, C^2), 134.1 (m, $C^{8/9}$), 133.7 (s, C^{10}), 130.5 (m, $C^{8/9}$), 125.6 (s, C^4), 123.8 (d, $^1J_{P\text{-}C}$ = 54.4 Hz, C^7), 122.1 (m, C^5), 34.8 (s, $C_{quat.tBu}$), 30.9 (s, $CH_{3\text{-}tBu}$). $^{31}P\{^1H\}$ NMR ($CDCl_3$, 121.5 MHz, 300 K): δ 55.4 (s, 2 P, P-Au), -144.3 (h, $^1J_{P\text{-}F}$ = 715 Hz, 1 P, PF_6). ESI-MS (MeCN) *positive mode exact mass for* $[C_{50}H_{48}P_2Au]^+$ (907.2891): measured *m/z* 907.2885 $[M\text{-}PF_6]^+$. Calcd for $C_{50}H_{48}P_2AuPF_6.3H_2O$ (1106.86): C, 54.26; H, 4.92. Found: C, 54.33; H 4.77.

Complex 2: *bis*(diphenylphosphino)methane (31 mg). The pure product is obtained as a pale yellow powder (67 mg, 0.068 mmol, 85% yield). ^{1}H NMR ($CDCl_3$, 300 MHz, 300 K): δ 7.78 (m, 8 H, H^9), 7.61-7.53 (m, 12 H, $H^8 + H^{10}$), 7.42 (m, 2 H, H^5), 7.24-7.21 (m, 4 H, $H^2 + H^4$), 5.17 (t, $^2J_{P\text{-}H}$ = 11.1 Hz, 2 H, H^{11}), 0.93 (s, 18 H, ^{t}Bu). $^{13}C\{^1H\}$ Jmod NMR (CD_3CN, 75.5 MHz, 300 K): δ 163.3 (d, $^2J_{P\text{-}C}$ = 116.1 Hz, C^6), 151.7 (s, C^1), 151.2 (m, C^3) 135.0 (d, $^2J_{P\text{-}C}$ = 12.4 Hz, $C^{8/9}$), 134.2 (t, $^3J_{P\text{-}C}$= 9.8 Hz, C^2), 131.9 (d, $^3J_{P\text{-}C}$= 12.1 Hz, $C^{8/9}$), 126.4 (s, C^4), 123.8 (d, $^1J_{P\text{-}C}$ = 52.5 Hz, C^7), 123.1 (m, C^5), 37.2 (t, $^2J_{P\text{-}C}$ = 30.2 Hz, C^{11}), 35.4 (s, $C_{quat.tBu}$), 31.2 (s, $CH_{3\text{-}tBu}$). $^{31}P\{^1H\}$ NMR ($CDCl_3$, 121.5 MHz): δ -7.7 (s, 2 P, P-Au), -144.6 (h, $^1J_{P\text{-}F}$ = 707 Hz, 1 P, PF_6). ESI-MS (MeCN)

positive mode exact mass for $[C_{45}H_{46}P_2Au]^+$ (845.2740): measured *m/z* 845.2738 $[M\text{-}PF_6]^+$. Calcd for $C_{45}H_{46}P_2AuPF_6$ (990.74): C, 54.55; H, 4.68. Found: C, 54.28; H 4.12.

Complex 3: 1,2-*bis*(diphenylphosphino)ethane (32 mg). The pure product is obtained as a pale yellow powder (57 mg, 0.057 mmol, 71% yield). ^{1}H NMR ($CDCl_3$, 300 MHz, 300 K): δ 7.79-7.85 (m, 8 H, H^9), 7.56-7.68 (m, 12 H, $H^8 + H^{10}$), 7.42 (dd, $^3J_{H\text{-}H}$= 7.7 Hz, $^5J_{P\text{-}H}$= 3.4 Hz, 2 H, H^5), 7.32 (dm, $^4J_{P\text{-}H}$= 10.6 Hz, 2 H, H^4), 7.17 (d, $^4J_{H\text{-}H}$= 8.2 Hz, 2 H, H^4), 3.00 (dm, $^2J_{P\text{-}H}$= 18.6 Hz, 4 H, H^{11}), 0.76 (s, 18 H, ^{t}Bu).^{13}C{^{1}H} Jmod NMR ($CDCl_3$, 75.5 MHz, 300 K): δ 162.9 (dd, $^2J_{P\text{-}C}$ = 111.6 Hz, $^2J_{P\text{-}C}$ = 6.8 Hz, C^6), 152.1 (m, C^1), 151.1 (m, C^3), 136.5 (m, C^2), 134.0 (m, $C^{8/9}$),133.8 (s, C^{10}), 130.6 (m, $C^{8/9}$), 125.3 (s, C^4), 123.0 (d, $^1J_{P\text{-}C}$ = 50.7 Hz, C^7), 121.8 (m, C^5), 34.8 (s, $C_{quat.tBu}$), 30.9 (s, $CH_{3\text{-}tBu}$), 29.4 (dd, $^1J_{P\text{-}C}$ = 37.0 Hz, $^2J_{P\text{-}C}$ = 7.4 Hz, C^{11}). ^{31}P{^{1}H} NMR ($CDCl_3$, 121.5 MHz): δ 59.6 (s, 2 P, P-Au), -144.3 (h, $^1J_{P\text{-}F}$ = 713 Hz, 1 P, PF_6). ESI-MS (MeCN) *positive mode exact mass for* $[C_{46}H_{48}P_2Au]^+$ (859.2897): measured *m/z* 859.2887 $[M\text{-}PF_6]^+$. Calcd for $C_{46}H_{48}P_2AuPF_6.0.5H_2O$ (1013.78): C, 54.50; H, 4.87. Found: C, 54.37; H 4.08.

Complex 4. 1,3-*bis*(diphenylphosphino)propane (33 mg). The pure product is obtained as a pale yellow powder (52 mg, 0.051 mmol, 64% yield). ^{1}H NMR ($CDCl_3$, 300 MHz, 300 K): δ 7.87-7.91 (m, 8 H, H^9), 7.56-7.64 (m, 12 H, $H^8 + H^{10}$), 7.36 (dd, $^3J_{H\text{-}H}$ = 8.0 Hz, $^5J_{P\text{-}H}$ = 3.6 Hz, 2 H, H^5), 7.14-7.18 (m, 2 H, H^2), 7.11 (dd, $^3J_{H\text{-}H}$ = 8.0 Hz, $^4J_{H\text{-}H}$ = 1.4 Hz, 2 H, H^4), 2.64-2.70 (m, 4 H, H^{11}), 2.28-2.41 (m, 2 H, H^{12}), 0.72 (s, 18 H, ^{t}Bu). ^{13}C{^{1}H} Jmod NMR ($CDCl_3$, 75.5 MHz, 300 K): δ 164.0 (dd, $^2J_{P\text{-}C}$ = 117.7 Hz, $^2J_{P\text{-}C}$ = 12.8 Hz, C^6), 152.2 (s, C^1), 150.5 (t, $^4J_{P\text{-}C}$ = 6.0 Hz, C^3), 135.5 (t, $^3J_{P\text{-}C}$= 8.3 Hz, C^2), 133.9 (t, $^4J_{P\text{-}C}$= 6.0 Hz, 5.3 Hz, C^5), 133.4 (s, C^{10}), 130.4 (t, $^4J_{P\text{-}C}$= 5.3 Hz, 6.0 Hz, $C^{8/9}$), 125.3 (s, C^4), 124.6 (d, $^2J_{P\text{-}C}$ = 11.3 Hz, $C^{8/9}$), 123.8 (d, $^2J_{P\text{-}C}$ = 11.3 Hz, C^7), 121.8 (t,

$^4J_{P\text{-}C}$= 3.0 Hz, C^{15}), 34.7 (s, $C_{quat.tBu}$), 30.9 (s, $CH_{3\text{-}tBu}$), 23.7 (t, $^2J_{P\text{-}C}$ = 21.9 Hz, C^{11}), 18.0 (s, C^{12}).$^{31}P\{^1H\}$ NMR ($CDCl_3$, 121.5 MHz, 300 K): δ 19.8 (s, 2 P, P-Au), -144.3 (h, $^1J_{P\text{-}F}$ = 713 Hz, 1 P, PF_6). ESI-MS (MeCN) *positive mode exact mass for* $[C_{46}H_{48}P_2Au]^+$ (873.3053): measured *m/z* 873.3052 $[M\text{-}PF_6]^+$. Calcd for $C_{47}H_{50}P_2AuPF_6$ (1018.79): C, 55.41; H, 4.95. Found: C, 55.49; H 4.32.

Complex 5: 1,4-bis(diphenylphosphino)butane (34 mg). The pure product is obtained as a pale yellow powder (59 mg, 0.057 mmol, 71 % yield). ^1H NMR ($CDCl_3$, 300 MHz, 300 K): δ 7.75-7.81 (m, 8 H, H^9), 7.34-7.50 (m, 14 H, $H^5 + H^8 + H^{10}$), 7.08-7.13 (m, 4 H, $H^2 + H^4$), 3.05 (s, 4 H, H^{12}), 2.05 (d, $^2J_{P\text{-}H}$ = 26.3 Hz, 4 H, H^{11}), 0.70 (s, 18 H, ^{t}Bu). $^{13}C\{^1H\}$ Jmod NMR (CD_3CN, 75.5 MHz, 300 K): δ 153.1 (s, C^1), 150.87 (t, $^4J_{P\text{-}C}$= 6.0 Hz, C^1), 135.8 (t, $^3J_{P\text{-}C}$= 8.3 Hz,$C^{3/6}$), 135.0 (t, $^4J_{P\text{-}C}$= 5.3 Hz, $C^{8/9}$), 133.7 (s, C^{10}), 130.7 (t, $^4J_{P\text{-}C}$ = 5.3 Hz, C^2), 129.1 (d, $^3J_{P\text{-}C}$= 8.3 Hz, $C^{8/9}$), 128.3 (d, $^3J_{P\text{-}C}$ = 8.3 Hz, C^4), 126.3 (s, C^7), 122.7 (t, $^4J_{P\text{-}C}$ = 3.0, C^5), 35.4 (s, $C_{quat.tBu}$), 31.0 (s, $CH_{3\text{-}tBu}$), 29.5 (d, $^1J_{P\text{-}C}$= 29.2 Hz, C^{11}), 23.9 (s, C^{12}). $^{31}P\{^1H\}$ NMR (CD_3CN, 121.5 MHz, 300 K): δ 35.3 (s, 2 P, P-Au), -144.6 (h, $^1J_{P\text{-}F}$ = 707 Hz, 1 P, PF_6). ESI-MS (MeCN) *positive mode exact mass for* $[C_{48}H_{52}P_2Au]^+$ (887.3210): measured *m/z* 887.321 $[M\text{-}PF_6]^+$. Calcd for $C_{48}H_{52}P_2AuPF_6.0.5H_2O$ (1041.79): C, 55.34; H, 5.13. Found: C, 55.10; H 4.51.

Synthesis of complexes 6

In a Schlenk tube under N_2 atmosphere, [(C^N)$AuCl_2$] (40 mg, 0.084 mmol) is suspended into degassed dichloromethane (5 mL). Diphenylphosphinoethane (33 mg, 0.084 mmol) is added and the reaction is kept under N_2 atmosphere at room temperature overnight. Silver hexafluorophosphate (42 mg, 0.168 mmol) is dissolved into degasses acetonitrile (1 mL), added

to the mixture and the reaction is kept under N_2 atmosphere at room temperature for 2 h. The reaction mixture was filtered through a glass frit with Celite and the obtained solution was concentrated under reduced pressure. Upon addition of a large amount of diethylether a white precipitate was formed which was recovered to give after drying the pure product as a white powder (90 mg, 0.082 mmol, 98% yield). ^{1}H NMR (CD_3CN, 400 MHz): δ 8.23 (dd, $^{3}J_{H\text{-}H}$ = 8.1 Hz, $^{5}J_{P\text{-}H}$ = 5.9 Hz, 1 H, H^5), 8.04 (ddd, $^{3}J_{H\text{-}H}$ = 8.1 Hz, $^{4}J_{H\text{-}H}$ = 1.7 Hz, $^{6}J_{P\text{-}H}$ = 1.7 Hz, 1 H, H^4), 7.96 (d, $^{3}J_{H\text{-}H}$ = 8.2 Hz, 1 H, H^8), 7.80 (ddd, $^{3}J_{H\text{-}H}$ = 8.2 Hz, $^{3}J_{H\text{-}H}$ = 7.4 Hz, $^{4}J_{H\text{-}H}$ = 1.2 Hz, 1 H, H^9), 7.74 (d, $^{3}J_{H\text{-}H}$ = 4.2 Hz, 1 H, H^{11}), 7.57-7.66 (m, 8 H, H_{oPh}), 7.48-751 (m, 12 H, H_{mPh} + H_{pPh}), 7.26 (dd, $^{4}J_{P\text{-}H}$ = 17.2 Hz, $^{4}J_{H\text{-}H}$ = 1.7 Hz, 1 H, H^2), 7.08 (dd, $^{3}J_{H\text{-}H}$ = 7.2 Hz, $^{3}J_{H\text{-}H}$ = 4.5 Hz, 1 H, H^{10}), 3.56-3.65 (m, 2 H, P-CH_2), 2.75-2.85 (m, 2 H, P-CH_2), 1.16 (s, 9 H, ^{t}Bu). $^{13}C\{^{1}H\}$ (CD_3CN, 150.9 MHz): δ 154.8 (d, $^{4}J_{P\text{-}C}$ = 12.3 Hz, C^3), 153.9 (s, C^7), 147.6 (s, C^{11}), 142.3 (d, $^{2}J_{P\text{-}C}$ = 3.8 Hz, C^1), 139.7 (s, C^9), 137.8 (d, $^{3}J_{P\text{-}C}$ = 13.8 Hz, C^3), 134.7 (d, $^{4}J_{P\text{-}C}$ = 2.7 Hz, $C^{15/15'}$), 134.5 (d, $^{2}J_{P\text{-}C}$ = 13.7 Hz, $C^{13/13'}$), 134.1 (d, $^{4}J_{P\text{-}C}$ = 2.3 Hz, C^4), 133.9 (d, $^{4}J_{P\text{-}C}$ = 2.7 Hz, $C^{15/15'}$), 132.8 (d, $^{2}J_{P\text{-}C}$ = 10.1 Hz, $C^{13/13'}$), 131.1 (d, $^{3}J_{P\text{-}C}$ = 8.1 Hz, C^5), 130.9 (d, $^{3}J_{P\text{-}C}$ = 12.2 Hz, $C^{14/14'}$), 130.7 (d, $^{3}J_{P\text{-}C}$ = 12.1 Hz, $C^{14/14'}$), 128.3 (d, $^{1}J_{P\text{-}C}$ = 62.2 Hz, $C^{12/12'}$), 125.3 (s, C^{10}), 125.1 (d, $^{1}J_{P\text{-}C}$ = 85.2 Hz, $C^{12/12'}$), 123.1 (s, C^8), 114.5 (d, $^{3}J_{P\text{-}C}$ = 93.3 Hz, C^6), 35.9 (s, $C_{quat.tBu}$), 30.9 (s, $CH_{3.tBu}$), 25.0 (dd, $^{1}J_{P\text{-}C}$ = 63.4 Hz, $^{2}J_{P\text{-}C}$ = 6.6 Hz, $C^{16/16'}$), 25.5 (dd, $^{1}J_{P\text{-}C}$ = 36.6 Hz, $^{2}J_{P\text{-}C}$ = 2.5 Hz, $C^{16/16'}$). $^{31}P\{^{1}H\}$ (CD_3CN, 121.5 MHz): δ 32.5 (d, $^{2}J_{P\text{-}P}$ = 67.1 Hz, 1 P, Ph_2PCH_2), 27.6 (d, $^{2}J_{P\text{-}P}$ = 67.1 Hz, 1 P, Ph_2PCH_2), -144.6 (h, $^{1}J_{P\text{-}F}$ = 704.8 Hz, 2 P, PF_6). ESI-MS (MeCN) *positive mode exact mass for* $[C_{41}H_{40}NP_2Au]^{2+}$ (402.6145): measured *m/z* 402.6140 $[M\text{-}2(PF_6)]^{2+}$. Calcd for $C_{41}H_{40}P_2NAu(PF_6)_2.2.5H_2O$ (1140.66): C, 43.17; H, 3.98; N, 1.23. Found: C, 43.14; H 3.61; N, 1.10.

Synthesis of complexes 7

In a Schlenk tube under N_2 atmosphere, [(C^N)Pt(DMSO)Cl] (40 mg, 0.077 mmol) is dissolved into degassed dichloromethane (4 mL). Diphenylphosphinoethane (31 mg, 0.077 mmol) is added and the reaction is kept under N_2 atmosphere at room temperature for 2 h. Silver hexafluorophosphate (19 mg, 0.077 mmol) is dissolved into degasses acetonitrile (1mL), added to the mixture and the reaction is kept under N_2 atmosphere at room temperature for 2 h. The reaction mixture was filtered through a glass frit with Celite and the obtained solution was concentrated under reduced pressure. Upon addition of a large amount of petroleum ether, a pale yellow precipitate was formed which was recovered, washed with Et_2O to give after drying the pure product as a pale yellow powder (71 mg, 0.075 mmol, 97% yield). ^{1}H NMR ($CDCl_3$, 400 MHz): δ 8.18 (t, $^3J_{H\text{-}H}$ = 4.8 Hz, 1 H, H^{11}), 7.92-7.98 (m, 6 H, H^8 + H^9 + 4 $H_{ortho\text{-}Ph}$), 7.79-7.83 (m, 4 H, $H_{para\text{-}Ph}$), 7.65 (dd, $^3J_{H\text{-}H}$ = 7.2 Hz, $^4J_{H\text{-}H}$ = 2.0 Hz, H^4), 7.50-7.61 (m, 12 H, 8 $H_{meta\text{-}Ph}$ + 4 $H_{ortho\text{-}Ph}$), 7.15-7.19 (m, 2 H, H^2 + H^5), 6.86-6.82 (m, 1 H, H^{10}), 2.42-2.60 (m, 4 H, $P(CH_2)_2P$), 0.77 (s, 9 H, ^{t}Bu). $^{13}C\{^1H\}$ Jmod NMR ($CDCl_3$, 75.5 MHz, 300 Hz): δ 168.0 (dd, $^3J_{P\text{-}C}$ = 5.6 Hz, $^3J_{P\text{-}C}$ = 1.9 Hz, C^7), 159.7 (dd, $^2J_{P\text{-}C}$ = 100.6 Hz, $^2J_{P\text{-}C}$ = 4.5 Hz, C^1), 154.6 (dd, $^4J_{P\text{-}C}$ = 6.6 Hz, $^4J_{P\text{-}C}$ = 2.3 Hz, C^3), 152.4 (d, $^3J_{P\text{-}C}$ = 7.3 Hz, C^{11}), 144.8 (s, C^6), 141.4 (s, C^8), 138.0 (dd, $^3J_{P\text{-}C}$ = 7.8 Hz, $^3J_{P\text{-}C}$ = 3.0 Hz, C^2), 133.8-134.3 (m, C_{mPh}), 132.8 (d, $^4J_{P\text{-}C}$ = 2.6 Hz, C_{pPh}), 130.1 (d, $^2J_{P\text{-}C}$ = 10.5 Hz, C_{oPh}), 129.7 (d, $^2J_{P\text{-}C}$ = 11.5 Hz, C_{oPh}), 126.9 (d, $^1J_{P\text{-}C}$ = 46.2 Hz, C_{iPh}), 125.7 (d, $^1J_{P\text{-}C}$ = 60.6 Hz, C_{iPh}), 124.4 (d, $^5J_{P\text{-}C}$ = 5.2 Hz, C^4), 124.0 (s, C^{10}), 123.2 (s, C^5), 120.3 (d, $^5J_{P\text{-}C}$ = 2.3 Hz, C^9), 34.9 (s, $C_{quat.tBu}$), 31.6 (dd, $^1J_{P\text{-}C}$ = 44.3 Hz, $^2J_{P\text{-}C}$ = 14.7 Hz, PCH_2), 30.8 (s, $CH_{3.tBu}$), 28.6 (dd, $^1J_{P\text{-}C}$ = 36.5 Hz, $^2J_{P\text{-}C}$ = 5.6 Hz, PCH_2). $^{31}P\{^1H\}$ ($CDCl_3$, 161.97 MHz): δ 50.9 (s + d, $^1J_{Pt\text{-}PtransC}$ = 1830 Hz, 1 P, P trans C), 41.7 (s + d, $^1J_{Pt\text{-}PtransN}$ = 3780 Hz, 1 P, P trans N), -144.3 (h, $^1J_{F\text{-}P}$ = 715 Hz, 1 P, PF_6^-). $^{195}Pt\{^1H\}$ ($CDCl_3$, 128.45 Hz): δ -4597 (dd, $^1J_{Pt\text{-}PtransN}$ = 3789 Hz, $^1J_{Pt\text{-}PtransC}$ = 1882 Hz, $[(C^N)Pt(P^P)]^+$). ESI-MS (MeCN) *positive mode exact mass for* $[C_{41}H_{40}NP_2Pt]^+$ (803.2278): measured *m/z*

803.2284 $[M\text{-}PF_6]^+$. Calcd for $C_{41}H_{40}P_2NPtPF_6$ (948.77): C, 51.90; H, 4.25; N, 1.48. Found: C, 51.85; H 4.50; N, 1.24.

X-ray diffractometric analysis

For each compound, a single crystal of each compound was selected, mounted onto a cryoloop and transferred into a cold nitrogen gas stream. Intensity data were collected with a Bruker Kappa APEX-II CCD diffractometer using a micro-focused Cu-Kα radiation (λ = 1.54178 Å) for **1PF6**, **2** and **7** or using a graphite-monochromated Mo-Kα radiation (λ = 0.71073 Å) for **1Cl**, **3**, **4** and **5**. Data collections were performed at 200K, with the Bruker APEXIII suite. Unit-cell parameters determinations, integrations and data reductions were carried out with SAINT program. SADABS was used for scaling and absorption corrections. The structures were solved with SHELXT[69] and refined by full-matrix least-squares methods with SHELXL[70] using Olex2 software package.[71] All non-hydrogen atoms were refined anisotropically. For complex **2**, large voids are present in the crystal lattice along the *b*-axis. In these channels, unattributed residual electron density is present, which should be due to very disordered solvent molecules. A PLATON SQUEEZE[72] procedure was applied to structure refinement to mask electron density of these very disordered solvent regions. Crystals were obtained with a mixture of dichloromethane, acetonitrile and petroleum ether, so it was impossible to identify and quantify which ones were present in the crystal. So, dichloromethane and/or hydrocarbon molecules could be also present in the crystal lattice.

The structures were deposited at the Cambridge Crystallographic Data Centre with numbers CCDC 2207307 to 2207313 and can be obtained free of charge via www.ccdc.cam.ac.uk.

Photophysics

Instrument details. Absorption spectra of fluid solution samples were measured on a Varian Cary 100 double-beam UV–VIS spectrophotometer and baseline corrected. Steady-state emission spectra were recorded on a Horiba Jobin−Yvon IBH FL-322 Fluorolog 3 spectrometer equipped with a 450 W xenon arc lamp, double-grating excitation, and emission monochromators (2.1 nm mm^{-1} of dispersion; 1200 grooves mm^{-1}) and a Hamamatsu R13456 red sensitive Peltier-cooled PMT detector. Emission and excitation spectra were corrected for source intensity (lamp and grating) and emission spectral response (detector and grating) by standard correction curves. Time-resolved measurements were performed using either the time-correlated single-photon counting (TCSPC) or the Multi Channel Scaling (MCS) electronics option of the TimeHarp 260 board installed on a PicoQuant FluoTime 300 fluorimeter (PicoQuant GmbH, Germany), equipped with a PDL 820 laser pulse driver. A pulsed laser diode LDH-P-C-375 (λ = 375 nm, pulse full width at half maximum FWHM <40 ps) or LDH-P-C-440B (λ = 440 nm, pulse full width at half maximum FWHM <80 ps) driven at repetition rate in the range 50 kHz–40 MHz) was used to excite the sample either with either single pulse or burst mode. Excitation source was mounted directly on the sample chamber at 90°. The photons were collected by a PMA Hybrid-07 single photon counting detector. The data were acquired by using the commercially available software EasyTau II (PicoQuant GmbH, Germany), while data analysis was performed using the built-in software FluoFit (PicoQuant GmbH, Germany). All the PLQYs on samples were recorded at a fixed excitation wavelength by using a Hamamatsu Photonics absolute PLQY measurements system Quantaurus QY equipped with CW Xenon light source (150 W), monochromator, integrating sphere, C7473 photonics multi-channel analyzer and employing the commercially available U6039-05 PLQY measurement software (Hamamatsu Photonics Ltd., Shizuoka, Japan). All

measurements were repeated five times at the excitation wavelength λ_{exc} = 450 nm, unless otherwise stated.

Methods. For time resolved measurements, data fitting was performed by employing the maximum likelihood estimation (MLE) methods and the quality of the fit was assessed by inspection of the reduced χ^2 function and of the weighted residuals. For multi-exponential decays, the intensity, namely I*(t)*, has been assumed to decay as the sum of individual single exponential decays (eqn. 4):

$$I(t) = \sum_{i=1}^{n} \alpha_i exp\left(-\frac{t}{\tau_i}\right) \qquad eqn.\,4$$

where τ_i are the decay times and α_i are the amplitude of the component at t = 0. In the tables, the percentages to the pre-exponential factors, α_i, are listed upon normalization. Intensity average lifetimes were calculated by using the following equation (eqn. 5):[51]

$$\bar{\tau} = \frac{a_1\tau_1^2 + a_2\tau_2^2}{a_1\tau_1 + a_2\tau_2} \qquad eqn.\,5$$

All the solvents were spectrophotometric grade. Deaerated samples were prepared by the freeze-pump-thaw technique by using a homemade quartz cuvette equipped with a Rotaflo® stopcock.

Thermal analysis

Thermogravimetric analyses were carried out on a Q50 systems from TA Instruments under air with a thermal scanning rate of 5°C min^{-1}.

Cyclic voltammetry

Cyclic voltammetry has been performed in acetonitrile containing 0.1M of $TBABF_4$. Complexes **1PF$_6$**, **3**, **6** and **7** were dissolved at a concentration of 10^{-3} M in the CV medium. Cyclic voltammetry measurements were carried out at room temperature using an AUTOLAB PGSTAT302N galvanostat potentiostat (Metrohm, Switzerland). Measurements were performed with a three-electrode setup comprising a graphite working electrode, a saturated calomel electrode (SCE) as the quasi-reference electrode, and a platinum counter-electrode.

Computational details

All calculations have been performed with ADF 2019[73] at DFT level of theory with B3LYP functional.[74] All atoms were described by the TZP basis set.[75] Van der Waals forces were introduced through Grimme's corrections.[76] Solvent (CH_3CN) was introduced through COSMO model.[77] Scalar relativistic ZORA Hamiltonian was employed.[78] All geometries were fully optimized and the absorption spectra computed on the computed stationary point by mean of TD-DFT.[79] Excited states structures were optimized the same way. Tamm Dancoff approximation were used to avoid triplet instability.[80] The nature of the excited state was determined by mean of THEODore analysis.[81]

Interconversion barriers for **1** and **3** were computed with GAUSSIAN 09 version D01[82] at DFT level of theory (B3LYP functional) through a triplet wavefunction. All atoms were described by the 6-31+G** basis set[83] except gold for which the SDD basis set was used with its associated pseudopotential.[84] Van der Waals forces were included through Grimme's corrections and the solvent (acetonitrile) was described by a PCM. All structures were fully optimized and the nature of the encountered stationary point checked by a vibrational analysis. Minima were characterized by a full set of real frequencies and transition state by one and only one imaginary frequency. Gibbs free energies were extracted from these frequency calculations. Emission energy were

computed by doing a single point energy calculation on the triplet state optimized structure with a closed shell singlet wavefunction.

LEC device fabrication and characterization

Standard clean and UV/ozone treatment of the indium-tin oxide (ITO) coated glass substrates were performed before device fabrication. After substrate cleaning, poly(3,4-ethylenedioxythiophene):poly(styrene sulfonate) (PEDOT:PSS) layers (40 nm) were spin-coated at 3500 rpm on these ITO/glass substrates. These samples were then baked at 150°C for 30 min in ambient air. The mixture of complex (either **1PF$_6$** or **3**) and [BMIM$^+$(PF$_6$)$^-$] in acetonitrile solution was spun on top of the PEDOT:PSS layer. The weight percentages of [BMIM$^+$(PF$_6$)$^-$] for the LECs based on complex **1PF$_6$** and **3** were 20 and 10 wt.%, respectively. The ionic liquid [BMIM$^+$(PF$_6$)$^-$] was added to provide additional mobile ions to shorten the device turn-on time. A lower concentration of [BMIM$^+$(PF$_6$)$^-$] was used in the LEC based on complex **3** to avoid phase separation of the mixed emissive layer. Various solution concentrations (40, 60, and 80 mg mL^{-1} for complex **1PF$_6$** and 80, 100, and 120 mg mL^{-1} for complex **3**) were employed in spin coating at 2000 rpm to fabricate different emissive-layer thicknesses for device performance optimization.[85] The thicknesses of the emissive layers were measured by ellipsometry. After depositing the emissive layers, the samples were baked at 60 °C for 8 hours in a vacuum oven to remove the residual solvent. Finally, a silver top contact was deposited by thermal evaporation in a vacuum chamber (*ca.* 10^{-6} torr). The EL emission properties of these LECs were measured by using source-measurement units (B2901A, Keysight) and a calibrated Si photodiode. The EL spectra of these LECs were measured with a calibrated fiber-optic spectrometer (USB2000+, Ocean Optics). To obtain the optimized device performance, the LECs employing complexes **1PF$_6$** and **3** were

measured under constant currents and constant voltages, respectively. Device measurements were performed in a nitrogen glove box to reduce the device degradation rate.

SUPPORTING INFORMATION

The Supporting Information is available free of charge

Crystallographic structures, additional absorption and emission data, thermogravimetric data, cyclic voltamogramms, additional computational data and NMR spectra (PDF).

AUTHOR INFORMATION

Corresponding Authors

Benoît Bertrand: Sorbonne Université, CNRS, Institut Parisien de Chimie Moléculaire (IPCM UMR 8232), F-75005 Paris, France

Orcid: 0000-0003-0542-4454

Email: benoit.bertrand@sorbonne-universite.fr

Matteo Mauro: Université de Strasbourg, CNRS, Institut de Physique et Chimie des Matériaux de Strasbourg, UMR 7504, 23 rue du Loess, 67034 Strasbourg, France

Orcid: 0000-0001-6393-8053

Email: mauro@unistra.fr

Hai-Ching Su: Institute of Lighting and Energy Photonics, National Yang Ming Chiao Tung University, Tainan 71150, Taiwan

Orcid: 0000-0003-1100-4712

Email: haichingsu@nycu.edu.tw

Authors

Jeannine Yang: Sorbonne Université, CNRS, Institut Parisien de Chimie Moléculaire (IPCM UMR 8232), F-75005 Paris, France

Valerio Giuso: Université de Strasbourg, CNRS, Institut de Physique et Chimie des Matériaux de Strasbourg, UMR 7504, 23 rue du Loess, 67034 Strasbourg, France

Min-Chih Hou: Institute of Lighting and Energy Photonics, National Yang Ming Chiao Tung University, Tainan 71150, Taiwan

Edwyn Remadna: Sorbonne Université, CNRS, Institut Parisien de Chimie Moléculaire (IPCM UMR 8232), F-75005 Paris, France

Jérémy Forté: Sorbonne Université, CNRS, Institut Parisien de Chimie Moléculaire (IPCM UMR 8232), F-75005 Paris, France

Christophe Gourlaouen: Université de Strasbourg, CNRS, Institut de Chimie de Strasbourg, UMR 7177, Laboratoire de Chimie Quantique, 4 rue Blaise Pascal, 67081 Strasbourg, France

Author Contributions

The manuscript was written through contributions of all authors. All authors have given approval to the final version of the manuscript. ‡These authors contributed equally to the work.

ACKNOWLEDGMENT

Sorbonne Université, the Université de Strasbourg and the CNRS are kindly acknowledged for financial support. M.M. gratefully acknowledges the French Agence Nationale de Recherche (ANR) for funding the grant ANR-21-CE29-0015 “ChirON”. This work was supported by the Higher Education Sprout Project of the National Yang Ming Chiao Tung University and Ministry

of Education (MOE), Taiwan. B.B. thanks the MS^{3}U platform for the HRMS analyses. C.G. thanks the computing center of the Université de Strasbourg for computing time. Benoît Heinrich is kindly acknowledged for the technical help with TGA analyses and melting point determinations.

ABBREVIATIONS

LEC, Light-emitting Electrochemical Cell; [BMIM][PF_6], 1-butyl-3-methylimidazolium hexafluorophosphate

REFERENCES

(1) Costa, R. D.; Ortí, E.; Bolink, H. J.; Monti, F.; Accorsi, G.; Armaroli, N. Luminescent Ionic Transition-Metal Complexes for Light-Emitting Electrochemical Cells. *Angew. Chem. Int. Ed.* **2012**, *51* (33), 8178–8211. https://doi.org/10.1002/anie.201201471.

(2) Meier, S. B.; Tordera, D.; Pertegás, A.; Roldán-Carmona, C.; Ortí, E.; Bolink, H. J. Light-Emitting Electrochemical Cells: Recent Progress and Future Prospects. *Mater. Today* **2014**, *17* (5), 217–223. https://doi.org/10.1016/j.mattod.2014.04.029.

(3) Fresta, E.; Costa, R. D. Beyond Traditional Light-Emitting Electrochemical Cells – a Review of New Device Designs and Emitters. *J. Mater. Chem. C* **2017**, *5* (23), 5643–5675. https://doi.org/10.1039/C7TC00202E.

(4) Su, H.; Chen, Y.; Wong, K. Recent Progress in White Light-Emitting Electrochemical Cells. *Adv. Funct. Mater.* **2020**, *30* (33), 1906898. https://doi.org/10.1002/adfm.201906898.

(5) Bai, R.; Meng, X.; Wang, X.; He, L. Blue-Emitting Iridium(III) Complexes for Light-Emitting Electrochemical Cells: Advances, Challenges, and Future Prospects. *Advanced Functional Materials* **2020**, *30* (33), 1907169. https://doi.org/10.1002/adfm.201907169.

(6) He, L.; Wang, X.; Duan, L. Enhancing the Overall Performances of Blue Light-Emitting Electrochemical Cells by Using an Electron-Injecting/Transporting Ionic Additive. *ACS Appl. Mater. Interfaces* **2018**, *10* (14), 11801–11809. https://doi.org/10.1021/acsami.8b00466.

(7) Pertegás, A.; Shavaleev, N. M.; Tordera, D.; Ortí, E.; Nazeeruddin, M. K.; Bolink, H. J. Host–Guest Blue Light-Emitting Electrochemical Cells. *J. Mater. Chem. C* **2014**, *2* (9), 1605–1611. https://doi.org/10.1039/C3TC31983K.

(8) Sun, R.; Liao, C.-T.; Su, H.-C. Effects of Incorporating Salts with Various Alkyl Chain Lengths on Carrier Balance of Light-Emitting Electrochemical Cells. *Org. Electr.* **2014**, *15* (11), 2885–2892. https://doi.org/10.1016/j.orgel.2014.08.031.

(9) Huang, P.-C.; Krucaite, G.; Su, H.-C.; Grigalevicius, S. Incorporating a Hole-Transport Material into the Emissive Layer of Solid-State Light-Emitting Electrochemical Cells to Improve Device Performance. *Phys. Chem. Chem. Phys.* **2015**, *17* (26), 17253–17259. https://doi.org/10.1039/C5CP02034D.

(10) Shavaleev, N. M.; Scopelliti, R.; Grätzel, M.; Nazeeruddin, M. K.; Pertegás, A.; Roldán-Carmona, C.; Tordera, D.; Bolink, H. J. Pulsed-Current versus Constant-Voltage Light-Emitting Electrochemical Cells with Trifluoromethyl-Substituted Cationic Iridium(III) Complexes. *J. Mater. Chem. C* **2013**, *1* (11), 2241. https://doi.org/10.1039/c3tc00808h.

(11) Ma, D.; Tsuboi, T.; Qiu, Y.; Duan, L. Recent Progress in Ionic Iridium(III) Complexes for Organic Electronic Devices. *Adv. Mater.* **2017**, *29* (3), 1603253. https://doi.org/10.1002/adma.201603253.
(12) Cebrián, C.; Mauro, M. Recent Advances in Phosphorescent Platinum Complexes for Organic Light-Emitting Diodes. *Beilstein J. Org. Chem.* **2018**, *14*, 1459–1481. https://doi.org/10.3762/bjoc.14.124.
(13) Bolink, H. J.; Coronado, E.; Costa, R. D.; Gaviña, P.; Ortí, E.; Tatay, S. Deep-Red-Emitting Electrochemical Cells Based on Heteroleptic Bis-Chelated Ruthenium(II) Complexes. *Inorg. Chem.* **2009**, *48* (9), 3907–3909. https://doi.org/10.1021/ic802433b.
(14) Mahoro, G. U.; Fernandez-Cestau, J.; Renaud, J.; Coto, P. B.; Costa, R. D.; Gaillard, S. Recent Advances in Solid-State Lighting Devices Using Transition Metal Complexes Exhibiting Thermally Activated Delayed Fluorescent Emission Mechanism. *Adv. Opt. Mater.* **2020**, *8* (16), 2000260. https://doi.org/10.1002/adom.202000260.
(15) Elie, M.; Sguerra, F.; Di Meo, F.; Weber, M. D.; Marion, R.; Grimault, A.; Lohier, J.-F.; Stallivieri, A.; Brosseau, A.; Pansu, R. B.; Renaud, J.-L.; Linares, M.; Hamel, M.; Costa, R. D.; Gaillard, S. Designing NHC–Copper(I) Dipyridylamine Complexes for Blue Light-Emitting Electrochemical Cells. *ACS Appl. Mater. Interfaces* **2016**, *8* (23), 14678–14691. https://doi.org/10.1021/acsami.6b04647.
(16) Slinker, J. D.; Gorodetsky, A. A.; Lowry, M. S.; Wang, J.; Parker, S.; Rohl, R.; Bernhard, S.; Malliaras, G. G. Efficient Yellow Electroluminescence from a Single Layer of a Cyclometalated Iridium Complex. *J. Am. Chem. Soc.* **2004**, *126* (9), 2763–2767. https://doi.org/10.1021/ja0345221.
(17) Henwood, A. F.; Zysman-Colman, E. A Comprehensive Review of Luminescent Iridium Complexes Used in Light-Emitting Electrochemical Cells (LEECs). In *Iridium(III) in Optoelectronic and Photonics Applications*; John Wiley & Sons, Ltd, 2017; pp 275–357. https://doi.org/10.1002/9781119007166.ch7.
(18) Cheng, C.-Y.; Wang, C.-W.; Cheng, J.-R.; Chen, H.-F.; Yeh, Y.-S.; Su, H.-C.; Chang, C.-H.; Wong, K.-T. Enhancing Device Efficiencies of Solid-State White Light-Emitting Electrochemical Cells by Employing Waveguide Coupling. *J. Mater. Chem. C* **2015**, *3* (22), 5665–5673. https://doi.org/10.1039/C5TC00765H.
(19) Lin, G.-R.; Cheng, J.-R.; Wang, C.-W.; Sarma, M.; Chen, H.-F.; Su, H.-C.; Chang, C.-H.; Wong, K.-T. Solid-State White Light-Emitting Electrochemical Cells Based on Scattering Red Color Conversion Layers. *J. Mater. Chem. C* **2015**, *3* (48), 12492–12498. https://doi.org/10.1039/C5TC02835C.
(20) Tang, S.; Sandström, A.; Lundberg, P.; Lanz, T.; Larsen, C.; van Reenen, S.; Kemerink, M.; Edman, L. Design Rules for Light-Emitting Electrochemical Cells Delivering Bright Luminance at 27.5 Percent External Quantum Efficiency. *Nat. Commun.* **2017**, *8* (1), 1190. https://doi.org/10.1038/s41467-017-01339-0.
(21) Chen, Y.-Z.; Luo, D.; Hsiang, C.-H.; Yi, R.-H.; Lin, C.-H.; Lu, C.-W.; Liu, S.-W.; Chang, C.-H.; Su, H.-C. Highly Efficient Blue and White Light-Emitting Electrochemical Cells Employing Substrates Containing Embedded Diffusive Layers. *Org. Electr.* **2020**, *77*, 105515. https://doi.org/10.1016/j.orgel.2019.105515.
(22) Lee, J. -K.; Yoo, D. S.; Handy, E. S.; Rubner, M. F. Thin Film Light Emitting Devices from an Electroluminescent Ruthenium Complex. *Appl. Phys. Lett.* **1996**, *69* (12), 1686–1688. https://doi.org/10.1063/1.117028.

(23) Lin, Y.-D.; Lu, C.-W.; Su, H.-C. Long-Wavelength Light-Emitting Electrochemical Cells: Materials and Device Engineering. *Chem. Eur. J.*, **2022**, *28*, e202202985. https://doi.org/10.1002/chem.202202985.
(24) Weber, K. T.; Karikis, K.; Weber, M. D.; Coto, P. B.; Charisiadis, A.; Charitaki, D.; Charalambidis, G.; Angaridis, P.; Coutsolelos, A. G.; Costa, R. D. Cunning Metal Core: Efficiency/Stability Dilemma in Metallated Porphyrin Based Light-Emitting Electrochemical Cells. *Dalton Trans.* **2016**, *45* (34), 13284–13288. https://doi.org/10.1039/C6DT02293F.
(25) Cinninger, L. M.; Bastatas, L. D.; Shen, Y.; Holliday, B. J.; Slinker, J. D. Luminescent Properties of a 3,5-Diphenylpyrazole Bridged Pt(II) Dimer. *Dalton Trans.* **2019**, *48* (26), 9684–9691. https://doi.org/10.1039/C9DT00795D.
(26) Shafikov, M. Z.; Tang, S.; Larsen, C.; Bodensteiner, M.; Kozhevnikov, V. N.; Edman, L. An Efficient Heterodinuclear Ir(III)/Pt(II) Complex: Synthesis, Photophysics and Application in Light-Emitting Electrochemical Cells. *J. Mater. Chem. C* **2019**, *7* (34), 10672–10682. https://doi.org/10.1039/C9TC02930C.
(27) Fuertes, S.; Mardegan, L.; Martínez, I.; Ventura, S.; Ara, I.; Tordera, D.; Bolink, H. J.; Sicilia, V. Green Light-Emitting Electrochemical Cells Based on Platinum(II) Complexes with a Carbazole-Appended Carbene Ligand. *J. Mater. Chem. C* **2022**, *10* (41), 15491–15500. https://doi.org/10.1039/D2TC02539F.
(28) Housecroft, C. E.; Constable, E. C. TADF: Enabling Luminescent Copper(I) Coordination Compounds for Light-Emitting Electrochemical Cells. *J. Mater. Chem. C* **2022**, *10* (12), 4456–4482. https://doi.org/10.1039/D1TC04028F.
(29) Zhang, Q.; Zhou, Q.; Cheng, Y.; Wang, L.; Ma, D.; Jing, X.; Wang, F. Highly Efficient Electroluminescence from Green-Light-Emitting Electrochemical Cells Based on CuI Complexes. *Adv. Functi. Mater.* **2006**, *16* (9), 1203–1208. https://doi.org/10.1002/adfm.200500691.
(30) Herrera, R. P.; Gimeno, M. C. Main Avenues in Gold Coordination Chemistry. *Chem. Rev.* **2021**, *121* (14), 8311–8363. https://doi.org/10.1021/acs.chemrev.0c00930.
(31) Bronner, C.; Wenger, O. S. Luminescent Cyclometalated Gold(III) Complexes. *Dalton Trans.* **2011**, *40* (46), 12409. https://doi.org/10.1039/c1dt10636h.
(32) Lu, Y.; Ma, X.; Chang, X.; Liang, Z.; Lv, L.; Shan, M.; Lu, Q.; Wen, Z.; Gust, R.; Liu, W. Recent Development of Gold(I) and Gold(III) Complexes as Therapeutic Agents for Cancer Diseases. *Chem. Soc. Rev.* **2022**, *51* (13), 5518–5556. https://doi.org/10.1039/D1CS00933H.
(33) Bertrand, B.; Williams, M. R. M.; Bochmann, M. Gold(III) Complexes for Antitumor Applications: An Overview. *Chem. Eur. J.* **2018**, *24* (46), 11840–11851. https://doi.org/10.1002/chem.201800981.
(34) Gil-Moles, M.; Basu, U.; Büssing, R.; Hoffmeister, H.; Türck, S.; Varchmin, A.; Ott, I. Gold Metallodrugs to Target Coronavirus Proteins: Inhibitory Effects on the Spike-ACE2 Interaction and on PLpro Protease Activity by Auranofin and Gold Organometallics. *Chem. Eur. J.* **2020**, *26* (66), 15140–15144. https://doi.org/10.1002/chem.202004112.
(35) Jouhannet, R.; Dagorne, S.; Blanc, A.; Frémont, P. Chiral Gold(III) Complexes: Synthesis, Structure, and Potential Applications. *Chem. Eur. J.* **2021**, *27* (36), 9218–9240. https://doi.org/10.1002/chem.202100415.
(36) Tang, M.-C.; Chan, A. K.-W.; Chan, M.-Y.; Yam, V. W.-W. Platinum and Gold Complexes for OLEDs. *Top. Curr. Chem. (Z)* **2016**, *374* (4), 46. https://doi.org/10.1007/s41061-016-0046-y.

(37) Yam, V. W.-W.; Choi, S. W.-K.; Lai, T.-F.; Lee, W.-K. Syntheses, Crystal Structures and Photophysics of Organogold(III) Diimine Complexes. *J. Chem. Soc., Dalton Trans.* **1993**, No. 6, 1001. https://doi.org/10.1039/dt9930001001.
(38) Au, V. K.-M.; Wong, K. M.-C.; Zhu, N.; Yam, V. W.-W. Luminescent Cyclometalated *N* -Heterocyclic Carbene-Containing Organogold(III) Complexes: Synthesis, Characterization, Electrochemistry, and Photophysical Studies. *J. Am. Chem. Soc.* **2009**, *131* (25), 9076–9085. https://doi.org/10.1021/ja9027692.
(39) Wong, K. M.-C.; Hung, L.-L.; Lam, W. H.; Zhu, N.; Yam, V. W.-W. A Class of Luminescent Cyclometalated Alkynylgold(III) Complexes: Synthesis, Characterization, and Electrochemical, Photophysical, and Computational Studies of [Au(C ^ N ^ C)(C∶CR)] (C ^ N ^ C = κ^3 C,N,C Bis-Cyclometalated 2,6-Diphenylpyridyl). *J. Am. Chem. Soc.* **2007**, *129* (14), 4350–4365. https://doi.org/10.1021/ja068264u.
(40) Zeineddine, A.; Estévez, L.; Mallet-Ladeira, S.; Miqueu, K.; Amgoune, A.; Bourissou, D. Rational Development of Catalytic Au(I)/Au(III) Arylation Involving Mild Oxidative Addition of Aryl Halides. *Nat. Commun.* **2017**, *8* (1), 565. https://doi.org/10.1038/s41467-017-00672-8.
(41) Chambrier, I.; Rocchigiani, L.; Hughes, D. L.; Budzelaar, P. M. H.; Bochmann, M. Thermally Stable Gold(III) Alkene and Alkyne Complexes: Synthesis, Structures, and Assessment of the *Trans* -Influence on Gold-Ligand Bond Enthalpies. *Chem. Eur. J.* **2018**, *24* (44), 11467–11474. https://doi.org/10.1002/chem.201802160.
(42) Bohan, P. T.; Toste, F. D. Well-Defined Chiral Gold(III) Complex Catalyzed Direct Enantioconvergent Kinetic Resolution of 1,5-Enynes. *J. Am. Chem. Soc.* **2017**, *139* (32), 11016–11019. https://doi.org/10.1021/jacs.7b06025.
(43) Reid, J. P.; Hu, M.; Ito, S.; Huang, B.; Hong, C. M.; Xiang, H.; Sigman, M. S.; Toste, F. D. Strategies for Remote Enantiocontrol in Chiral Gold(III) Complexes Applied to Catalytic Enantioselective γ,δ-Diels–Alder Reactions. *Chem. Sci.* **2020**, *11* (25), 6450–6456. https://doi.org/10.1039/D0SC00497A.
(44) David, B.; Monkowius, U.; Rust, J.; Lehmann, C. W.; Hyzak, L.; Mohr, F. Gold(III) Compounds Containing a Chelating, Dicarbanionic Ligand Derived from 4,4′-Di- *Tert* -Butylbiphenyl. *Dalton Trans.* **2014**, *43* (28), 11059–11066. https://doi.org/10.1039/C4DT00778F.
(45) Chan, K. T.; Tong, G. S. M.; Wan, Q.; Cheng, G.; Yang, C.; Che, C.-M. Strongly Luminescent Cyclometalated Gold(III) Complexes Supported by Bidentate Ligands Displaying Intermolecular Interactions and Tunable Emission Energy. *Chem. Asian J.* **2017**, *12* (16), 2104–2120. https://doi.org/10.1002/asia.201700686.
(46) Garg, J. A.; Blacque, O.; Fox, T.; Venkatesan, K. Stable and Tunable Phosphorescent Neutral Cyclometalated Au(III) Diaryl Complexes. *Inorg. Chem.* **2010**, *49* (24), 11463–11472. https://doi.org/10.1021/ic101437h.
(47) Khodjoyan, S.; Remadna, E.; Dossmann, H.; Lesage, D.; Gontard, G.; Forté, J.; Hoffmeister, H.; Basu, U.; Ott, I.; Spence, P.; Waller, Z. A. E.; Salmain, M.; Bertrand, B. [(C C)Au(N N)]+ Complexes as a New Family of Anticancer Candidates: Synthesis, Characterization and Exploration of the Antiproliferative Properties. *Chem. Eur. J.* **2021**, *27* (63), 15773–15785. https://doi.org/10.1002/chem.202102751.
(48) Rothe, C.; Chiang, C.-J.; Jankus, V.; Abdullah, K.; Zeng, X.; Jitchati, R.; Batsanov, A. S.; Bryce, M. R.; Monkman, A. P. Ionic Iridium(III) Complexes with Bulky Side Groups for Use

in Light Emitting Cells: Reduction of Concentration Quenching. *Adv. Funct. Mater.* **2009**, *19* (13), 2038–2044. https://doi.org/10.1002/adfm.200801767.
(49) Cinellu, M. A.; Zucca, A.; Stoccoro, S.; Minghetti, G.; Manassero, M.; Sansoni, M. Synthesis and Characterization of Gold(Iii) Adducts and Cyclometallated Derivatives with 2-Substituted Pyridines. Crystal Structure of [Au{NC5H4(CMe,C,H4)-2}C12]t. *J. Chem. Soc. Dalton Trans.* **1995**, 2865–2872. https://doi.org/10.1039/DT9950002865.
(50) Haghighi, M. G.; Nabavizadeh, S. M.; Rashidi, M.; Kubicki, M. Selectivity in Metal–Carbon Bond Protonolysis in p-Tolyl- (or Methyl)-Cycloplatinated(Ii) Complexes: Kinetics and Mechanism of the Uncatalyzed Isomerization of the Resulting Pt(Ii) Products. *Dalton Trans.* **2013**, *42* (37), 13369. https://doi.org/10.1039/c3dt51339d.
(51) Montalti, M.; Credi, A.; Prodi, L.; Gandolfi, M. T. *Handbook of Photochemistry*, 3rd ed.; CRC Press: Boca Raton, 2006. https://doi.org/10.1201/9781420015195.
(52) Lu, W.; Chan, K. T.; Wu, S.-X.; Chen, Y.; Che, C.-M. Quest for an Intermolecular Au(III)···Au(III) Interaction between Cyclometalated Gold(III) Cations. *Chem. Sci.* **2012**, *3* (3), 752–755. https://doi.org/10.1039/C2SC00947A.
(53) To, W.-P.; Tong, G. S. M.; Cheung, C.-W.; Yang, C.; Zhou, D.; Che, C.-M. Luminescent Cyclometalated Gold(III) Alkyl Complexes: Photophysical and Photochemical Properties. *Inorg. Chem.* **2017**, *56* (9), 5046–5059. https://doi.org/10.1021/acs.inorgchem.7b00180.
(54) Currie, L.; Fernandez-Cestau, J.; Rocchigiani, L.; Bertrand, B.; Lancaster, S. J.; Hughes, D. L.; Duckworth, H.; Jones, S. T. E.; Credgington, D.; Penfold, T. J.; Bochmann, M. Luminescent Gold(III) Thiolates: Supramolecular Interactions Trigger and Control Switchable Photoemissions from Bimolecular Excited States. *Chem. Eur. J.* **2017**, *23* (1), 105–113. https://doi.org/10.1002/chem.201603841.
(55) Hsu, J.-H.; Su, H.-C. Host-Only Solid-State Near-Infrared Light-Emitting Electrochemical Cells Based on Interferometric Spectral Tailoring. *Phys. Chem. Chem. Phys.* **2016**, *18* (6), 5034–5039. https://doi.org/10.1039/C5CP07065A.
(56) Su, H.-C. Optical Techniques for Light-Emitting Electrochemical Cells. *ChemPlusChem* **2018**, *83* (4), 197–210. https://doi.org/10.1002/cplu.201700455.
(57) Yang, Z.; Su, H. Recent Advances in Optical Engineering of Light-Emitting Electrochemical Cells. *Adv. Funct. Mater.* **2020**, *30* (33), 1906788. https://doi.org/10.1002/adfm.201906788.
(58) van Reenen, S.; Janssen, R. A. J.; Kemerink, M. Fundamental Tradeoff between Emission Intensity and Efficiency in Light-Emitting Electrochemical Cells. *Adv. Funct. Mater.* **2015**, *25* (20), 3066–3073. https://doi.org/10.1002/adfm.201403945.
(59) Yi, R.-H.; Lo, C.-L.; Luo, D.; Lin, C.-H.; Weng, S.-W.; Lu, C.-W.; Liu, S.-W.; Chang, C.-H.; Su, H.-C. Combinational Approach To Realize Highly Efficient Light-Emitting Electrochemical Cells. *ACS Appl. Mater. Interfaces* **2020**, *12* (12), 14254–14264. https://doi.org/10.1021/acsami.9b23300.
(60) Su, Y.-H.; Ji, Y.-C.; Huang, Y.-T.; Luo, D.; Liu, S.-W.; Yang, Z.-P.; Lu, C.-W.; Chang, C.-H.; Su, H.-C. Deep-Red and near-Infrared Light-Emitting Electrochemical Cells Employing Perovskite Color Conversion Layers with EQE >10%. *J. Mater. Chem. C* **2022**, *10* (48), 18137–18146. https://doi.org/10.1039/D2TC03813G.
(61) Fresta, E.; Volpi, G.; Milanesio, M.; Garino, C.; Barolo, C.; Costa, R. D. Novel Ligand and Device Designs for Stable Light-Emitting Electrochemical Cells Based on Heteroleptic Copper(I) Complexes. *Inorg. Chem.* **2018**, *57* (16), 10469–10479. https://doi.org/10.1021/acs.inorgchem.8b01914.

(62) Mahoro, G. U.; Fresta, E.; Elie, M.; di Nasso, D.; Zhang, Q.; Lohier, J.-F.; Renaud, J.-L.; Linares, M.; Wannemacher, R.; Cabanillas-Gonzalez, J.; Costa, R. D.; Gaillard, S. Towards Rainbow Photo/Electro-Luminescence in Copper(I) Complexes with the Versatile Bridged Bis-Pyridyl Ancillary Ligand. *Dalton Trans.* **2021**, *50* (32), 11049–11060. https://doi.org/10.1039/D1DT01689J.
(63) Keller, S.; Prescimone, A.; Bolink, H.; Sessolo, M.; Longo, G.; Martínez-Sarti, L.; Junquera-Hernández, J. M.; Constable, E. C.; Ortí, E.; Housecroft, C. E. Luminescent Copper(I) Complexes with Bisphosphane and Halogen-Substituted 2,2′-Bipyridine Ligands. *Dalton Trans.* **2018**, *47* (40), 14263–14276. https://doi.org/10.1039/C8DT01338A.
(64) Li, C.; Mackenzie, C. F. R.; Said, S. A.; Pal, A. K.; Haghighatbin, M. A.; Babaei, A.; Sessolo, M.; Cordes, D. B.; Slawin, A. M. Z.; Kamer, P. C. J.; Bolink, H. J.; Hogan, C. F.; Zysman-Colman, E. Wide-Bite-Angle Diphosphine Ligands in Thermally Activated Delayed Fluorescent Copper(I) Complexes: Impact on the Performance of Electroluminescence Applications. *Inorg. Chem.* **2021**, *60* (14), 10323–10339. https://doi.org/10.1021/acs.inorgchem.1c00804.
(65) Pashaei, B.; Karimi, S.; Shahroosvand, H.; Pilkington, M. Molecularly Engineered Near-Infrared Light-Emitting Electrochemical Cells. *Adv. Funct. Mater.* **2020**, *30* (33), 1908103. https://doi.org/10.1002/adfm.201908103.
(66) Shahroosvand, H.; Abaspour, S.; Pashaei, B.; Radicchi, E.; De Angelis, F.; Bonaccorso, F. A Ruthenium Tetrazole Complex-Based High Efficiency near Infrared Light Electrochemical Cell. *Chem. Commun.* **2017**, *53* (46), 6211–6214. https://doi.org/10.1039/C7CC02878D.
(67) Constable, E. C.; Leese, T. A. Cycloaurated Derivatives of 2-Phenylpyridine. *J. Organomet. Chem.* **1989**, *363* (3), 419–424. https://doi.org/10.1016/0022-328X(89)87129-3.
(68) Godbert, N.; Pugliese, T.; Aiello, I.; Bellusci, A.; Crispini, A.; Ghedini, M. Efficient, Ultrafast, Microwave-Assisted Syntheses of Cycloplatinated Complexes. *Eur. J. Inorg. Chem.* **2007**, *2007* (32), 5105–5111. https://doi.org/10.1002/ejic.200700639.
(69) Palatinus, L.; Chapuis, G. *SUPERFLIP* – a Computer Program for the Solution of Crystal Structures by Charge Flipping in Arbitrary Dimensions. *J Appl Crystallogr* **2007**, *40* (4), 786–790. https://doi.org/10.1107/S0021889807029238.
(70) Sheldrick, G. M. Crystal Structure Refinement with SHELXL. *Acta Cryst. C* **2015**, *71*, 3–8. https://doi.org/10.1107/S2053229614024218.
(71) Dolomanov, O. V.; Bourhis, L. J.; Gildea, R. J.; Howard, J. A. K.; Puschmann, H. OLEX2: A Complete Structure Solution, Refinement and Analysis Program. *J. Appl. Cryst.* **2009**, *42*, 339–341. https://doi.org/10.1107/S0021889808042726.
(72) Spek, A. L. PLATON SQUEEZE: A Tool for the Calculation of the Disordered Solvent Contribution to the Calculated Structure Factors. *Acta Cryst. C* **2015**, *71*, 9–18. https://doi.org/10.1107/S2053229614024929.
(73) *Amsterdam Modeling Suite Making Computational Chemistry Work For You*. Software for Chemistry & Materials. https://www.scm.com/ (accessed 2022-11-20).
(74) Becke, A. D. Density-functional Thermochemistry. III. The Role of Exact Exchange. *J. Chem. Phys.* **1993**, *98* (7), 5648–5652. https://doi.org/10.1063/1.464913.
(75) van Lenthe, E.; Baerends, E. J. Optimized Slater-type Basis Sets for the Elements 1–118. *J. Comput. Chem* **2003**, *24* (9), 1142–1156. https://doi.org/10.1002/jcc.10255.
(76) Grimme, S. Semiempirical GGA-type density functional constructed with a long-range dispersion correction. *Journal of Computational Chemistry* **2006**, *27* (15), 1787–1799. https://doi.org/10.1002/jcc.20495.

(77) Klamt, A. Conductor-like Screening Model for Real Solvents: A New Approach to the Quantitative Calculation of Solvation Phenomena. *J. Phys. Chem.* **1995**, *99*, 2224–2235. https://doi.org/10.1021/j100007a062.
(78) van Lenthe, E.; van Leeuwen, R.; Baerends, E. J.; Snijders, J. G. Relativistic regular two-component Hamiltonians. *Int. J. Quantum Chem.* **1996**, *57* (3), 281–293. https://doi.org/10.1002/(SICI)1097-461X(1996)57:3<281::AID-QUA2>3.0.CO;2-U.
(79) Gloor, G. J.; Jackson, G.; Blas, F. J.; de Miguel, E. Test-Area Simulation Method for the Direct Determination of the Interfacial Tension of Systems with Continuous or Discontinuous Potentials. *J. Chem. Phys.* **2005**, *123* (13), 134703. https://doi.org/10.1063/1.2038827.
(80) Peach, M. J. G.; Tozer, D. J. Overcoming Low Orbital Overlap and Triplet Instability Problems in TDDFT. *J. Phys. Chem. A* **2012**, *116* (39), 9783–9789. https://doi.org/10.1021/jp308662x.
(81) Plasser, F. TheoDORE: A Toolbox for a Detailed and Automated Analysis of Electronic Excited State Computations. *J. Chem. Phys.* **2020**, *152* (8), 084108. https://doi.org/10.1063/1.5143076.
(82) Frisch, M. J.; Trucks, G. W.; Schlegel, H. B.; Scuseria, G. E.; Robb, M. A.; Cheeseman, J. R.; Scalmani, G.; Baronne, V.; Mennucci, B.; Petersson, G. A.; Nakatsuji, H.; Caricato, M.; Li, X.; Hratchian, H. P.; Izmaylov, A. F.; Bloino, J.; Zheng, G.; Sonnenberg, J. L.; Hada, M.; Ehara, M.; Toyota, K.; Fukuda, R.; Hasegawa, J.; Ishida, M.; Nakajima, T.; Honda, Y.; Kitao, O.; Nakai, H.; Vreven, T.; Montgomery, Jr., J. A.; Peralta, J. E.; Ogliaro, F.; Bearpark, M.; Heyd, J. J.; Brothers, E.; Kudin, K. N.; Staroverov, V. N.; Kobayashi, R.; Normand, J.; Raghavachari, K.; Rendell, A.; Burant, J. C.; Iyengar, S. S.; Tomasi, J.; Cossi, M.; Rega, N.; Millam, J. M.; Klene, M.; Knox, J. E.; Cross, J. B.; Bakken, V.; Adamo, C.; Jaramillo, J.; Gomperts, R.; Stratmann, R. E.; Yazyev, O.; Austin, A. J.; Cammi, R.; Pomelli, C.; Ochterski, J. W.; Martin, R. L.; Morokuma, K.; Zakrzewski, V. G.; Voth, G. H.; Salvador, P.; Dannenberg, J. J.; Dapprich, S.; Daniels, A. D.; Farkas, Ö.; Foresman, J. B.; Ortiz, J. V.; Cioslowski, J.; Fox, D. J. Gaussian 09, Revision D.01, 2016.
(83) Hehre, W. J.; Ditchfield, R.; Pople, J. A. Self—Consistent Molecular Orbital Methods. XII. Further Extensions of Gaussian—Type Basis Sets for Use in Molecular Orbital Studies of Organic Molecules. *J. Chem. Phys.* **1972**, *56* (5), 2257–2261. https://doi.org/10.1063/1.1677527.
(84) Schwerdtfeger, P.; Dolg, M.; Schwarz, W. H. E.; Bowmaker, G. A.; Boyd, P. D. W. Relativistic Effects in Gold Chemistry. I. Diatomic Gold Compounds. *J. Chem. Phys.* **1989**, *91* (3), 1762–1774. https://doi.org/10.1063/1.457082.
(85) Bonfiglio, A.; Hsiao, P.-W.; Chen, Y.; Gourlaouen, C.; Marchand, Q.; César, V.; Bellemin-Laponnaz, S.; Wang, Y.-X.; Lu, C.-W.; Daniel, C.; Polo, F.; Su, H.-C.; Mauro, M. Highly Emissive Red Heterobimetallic Ir^{III}/M^{I} (M^{I} = Cu^{I} and Au^{I}) Complexes for Efficient Light-Emitting Electrochemical Cells. *Chem. Mater.* **2022**, *34* (4), 1756–1769. https://doi.org/10.1021/acs.chemmater.1c03972.

For Table of Contents Only

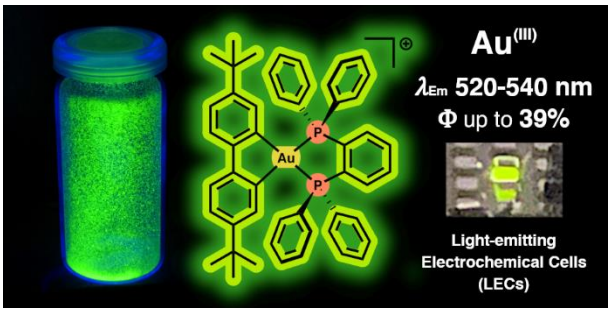

Synopsis

Biphenyl Au(III) diphosphine complexes present strong photoluminescence in solid state with quantum yield up to 39%. This strong emission rises from the rigidification of the systems in solid state preventing non-radiative decay. Some complexes were used for the fabrication of light-emitting electrochemical cells (LECs) with external quantum efficiency (EQE) of 1%. This represents the first proof-of-concept of the use of Au(III) complexes in LEC devices.